

# Possible evolution of the circum-galactic medium around QSOs with QSO age and cosmic time revealed by Ly $\alpha$ halos

Rieko Momose<sup>1,2</sup>, Tomotsugu Goto<sup>2</sup>, Yousuke Utsumi<sup>3</sup>, Tetsuya Hashimoto<sup>2</sup>, Chia-Ying Chiang<sup>2</sup>, Seong-Jin Kim<sup>2</sup>, Nobunari Kashikawa<sup>1</sup>, Kazuhiro Shimasaku<sup>1,4</sup>, Satoshi Miyazaki<sup>5</sup>

<sup>1</sup> Department of Astronomy, School of Science, The University of Tokyo, 7-3-1 Hongo, Bunkyo-ku, Tokyo 113-0033, JAPAN

<sup>2</sup> Institute of Astronomy, National Tsing Hua University, 101, Section 2 Kuang-Fu Road, Hsinchu, Taiwan, 30013

<sup>3</sup> Kavli Institute for Particle Astrophysics and Cosmology (KIPAC), SLAC National Accelerator Laboratory, Stanford University, 2575 Sand Hill Road, Menlo Park, CA 94025, USA

<sup>4</sup> Research Center for the Early Universe, The University of Tokyo, 7-3-1 Hongo, Bunkyo-ku, Tokyo 113-0033, Japan

<sup>5</sup> National Astronomical Observatory of Japan, 2-21-1 Osawa, Mitaka, Tokyo 181-8588, Japan

## ABSTRACT

We first present new Subaru narrow-band observations of the Ly $\alpha$  halo around the quasi-stellar object (QSO) CFHQ J232908–030158 at  $z = 6.42$ , which appears the most luminous and extended halo at  $z > 5$  ( $L_{\text{Ly}\alpha} = 9.8 \times 10^{43}$  erg s<sup>−1</sup> within 37 pkpc diameter). Then, combining these measurements with available data in the literature, we find two different evolutions of QSOs’ Ly $\alpha$  halos. First is a possible short-term evolution with QSO age seen in four  $z > 6$  QSOs. We find the anti-correlation between the Ly $\alpha$  halo scales with QSOs IR luminosity, with J2329–0301’s halo being the brightest and largest. It indicates that ionizing photons escape more easily out to circum-galactic regions when host galaxies are less dusty. We also find a positive correlation between IR luminosity and black hole mass ( $M_{\text{BH}}$ ). Given  $M_{\text{BH}}$  as an indicator of QSO age, we propose a hypothesis that a large Ly $\alpha$  halo mainly exists around QSOs in the young phase of their activity due to a small amount of dust. The second is an evolution with cosmic time seen over  $z \sim 2 - 5$ . We find the increase of surface brightness toward lower-redshift with a similar growth rate to that of dark matter halos (DHs) which evolve to  $M_{\text{DH}} = 10^{12} - 10^{13} M_{\odot}$  at  $z = 2$ . The extent of Ly $\alpha$  halos is also found to increase at a rate scaling with the virial radius of growing DHs,  $r_{\text{vir}} \propto M_{\text{DH}}^{1/3} (1+z)^{-1}$ . These increases are consistent with a scenario that the CGM around QSOs evolves in mass and size keeping pace with hosting DHs.

**Key words:** galaxies: haloes – galaxies: high-redshift – galaxies: evolution – quasars: general – quasars: individual: J2329-0301

## 1 INTRODUCTION

Gas exchanges between galaxies and the inter-galactic medium (IGM) around them play a central role in star formation and galaxy evolution. While the star formation activity of galaxies is maintained by gas inflows from the IGM (e.g., Dekel et al. 2009b,a), outflows induced by star formation heat or even blow away the cold gas in galaxies, thereby suppressing subsequent star formation (e.g., Mori et al. 2002, 2004; Scannapieco et al. 2005; Mori & Umemura 2006; Davé et al. 2011). Since inflow and outflow gas passing through or reaching circum-galactic regions makes up the circum-galactic medium (CGM) extending over up to a few hundred physical kpc (pkpc), physical properties of the

CGM such as mass and spatial extent provide valuable insights into star formation and galaxy evolution.

To understand the physical properties of the CGM, absorption lines are often used as a tracer of the cold gas phase of the CGM (e.g., Hennawi et al. 2006; Prochaska & Hennawi 2009; Hennawi & Prochaska 2013; Bouché et al. 2013, 2016; Prochaska et al. 2017). These studies have shown the presence of cold ( $T \sim 10^4$  K) and metal-enriched ( $Z > 0.1 Z_{\odot}$ ) gas extending to a few hundred pkpc (e.g., Hennawi & Prochaska 2013; Prochaska et al. 2013a, 2014; Farina et al. 2013, 2014; Johnson et al. 2015; Lau et al. 2016). Additionally, systemic surveys targeting pair QSOs (Quasars Probing Quasars) have also indicated optically thick H I gas in the CGM (e.g., Prochaska et al. 2014). Although these previous studies have found several

important properties of the CGM around galaxies, they have not provided full spatial distributions of the CGM because absorption lines usually provide parameters of one dimensional nature.

Another tracer is the emission lines from the CGM, among which the strongest is the hydrogen Ly $\alpha$ . If neutral hydrogen gas constituting the CGM gas is illuminated by ionizing or Ly $\alpha$  radiation produced in the hosting galaxy by star formation or AGN activities, it can be observed as a diffuse, extended Ly $\alpha$  halo (or called a Ly $\alpha$  nebula). Good examples are seen in Ly $\alpha$  emitters (LAEs), galaxies with strong Ly $\alpha$  emission. LAEs are known to possess Ly $\alpha$  halos with scale lengths reaching  $\sim 10$  pkpc independent of redshift (for studies based on stacking analysis, see, e.g., Steidel et al. 2011; Matsuda et al. 2012; Feldmeier et al. 2013; Momose et al. 2014, 2016; for individual-basis studies, see, e.g., Rauch et al. 2008; Wisotzki et al. 2016; Leclercq et al. 2017).

Quasi-stellar objects (QSOs) have brighter Ly $\alpha$  halos than normal galaxies, making it possible to detect them on an individual basis especially at  $z \sim 2 - 3$  (e.g. Heckman et al. 1991a,b; Christensen et al. 2006; North et al. 2012; Hennawi & Prochaska 2013; Roche et al. 2014; Borisova et al. 2016; Fathivavsari et al. 2016). Recently, the discovery of extremely giant Ly $\alpha$  halos over  $> 300$  pkpc has been reported (e.g., Cantalupo et al. 2014; Martin et al. 2014; Hennawi et al. 2015; Borisova et al. 2016; Cai et al. 2017; Arrigoni Battaia et al. 2018). Cantalupo et al. (2014) have detected a giant Ly $\alpha$  halo, named Slug Nebula, with an extent of  $\sim 460$  pkpc around a QSO at  $z = 2.28$ . This halo extends beyond the virial radius of the associated dark matter halo, indicating that Ly $\alpha$  emission of such a giant nebula also traces the IGM gas. Hennawi et al. (2015) have also discovered a giant Ly $\alpha$  halo of 310 pkpc extent covering four QSOs. These extremely extended Ly $\alpha$  halos indicate the presence of a widely spread CGM, and/or a large amount of cold gas around QSOs. However, at least at  $z \sim 3$ , QSOs' Ly $\alpha$  halos seem to have similar surface brightness (SB) profiles despite different luminosities and sizes. Borisova et al. (2016) have found that the SB profile of the Slug Nebula is consistent with the mean SB profile of Ly $\alpha$  halos around  $17 z \sim 3$  QSOs. Such similarity of SB profiles indicates that QSOs' Ly $\alpha$  halos have the same origin.

Observational studies of QSOs' Ly $\alpha$  halos have revealed another important trend, evolution with cosmic time, although based on samples over a relatively narrow redshift range of  $z \sim 2 - 4$  and with different SB limits. North et al. (2012) have found that the SBs of Ly $\alpha$  halos at  $z \sim 4.5$  are 1 – 2 order of magnitude fainter than those at  $z \sim 2 - 3$ . Ginolfi et al. (2018) have found that halos at  $z \sim 5$  are smaller than at  $z \sim 3 - 4$ . Moreover, Farina et al. (2017) have suggested a decline in the total Ly $\alpha$  luminosity of halos with redshift over  $2 < z < 7$  due to a change in gas properties and/or powering mechanisms of Ly $\alpha$  radiation. On the other hand, Arrigoni Battaia et al. (2019) have found an opposite trend (North et al. 2012; Farina et al. 2017; Ginolfi et al. 2018) that the mean SB of radio-quiet QSOs increases with redshift from  $z = 2$  to  $z = 3$ . Furthermore, no evolution has been found in the Ly $\alpha$  halos luminosity over  $2 < z < 4.5$  (Fathivavsari et al. 2016). These discrepancies may be attributed to different methodologies (e.g., SB limits, observa-

tion methods [spectroscopy or imaging], methods to measure sizes) in the literature. Hence, in order to comprehensively understand the properties and evolution of QSO Ly $\alpha$  halos, an analysis with a large sample compiled under the same conditions is required.

In addition, the number of observations for  $z > 6$  QSO halos is still limited. Goto et al. (2009) have for the first time reported a possible presence of a Ly $\alpha$  halo around a  $z > 6$  QSO, CFHQ J232908–030158 (hereafter J2329–0301) at  $z = 6.4$ , by showing an extended feature in a  $z'$ -band image whose bandpass covers Ly $\alpha$ , while detecting no such feature in other bands ( $i'$  and  $z_r$ -bands). After subtracting the PSF component from the QSO, they have confirmed residual emission of  $4''$ -wide corresponding to  $\sim 22$  pkpc around the QSO. On the other hand, Decarli et al. (2012) have not detected an extended Ly $\alpha$  halo around two QSOs at  $z = 6.3$  and  $6.4$  in spite of using deep Hubble Space Telescope images. Furthermore, Farina et al. (2017) have found a small and faint Ly $\alpha$  halo with 9 pkpc extent around the QSO J0305–3150 at  $z = 6.61$  even using a high sensitivity of Multi-Unit Spectroscopic Explorer (MUSE: Bacon et al. 2015). These studies imply a possible absence of large Ly $\alpha$  halos at  $z > 6$ , which may be attributed to the evolution of the CGM and/or some physical properties of QSOs.

In this paper, we first present new narrow-band observations of the Ly $\alpha$  halo around the QSO J2329–0301 at  $z = 6.4164$  (by [C II]  $\lambda_{\text{rest}} = 157.741 \mu\text{m}$ : Willott et al. 2017). Previous studies based on spectroscopic data have confirmed the presence of an extended Ly $\alpha$  halo with  $> 15$  pkpc wide (Goto et al. 2009, 2012; Willott et al. 2011), but the reported extent and total Ly $\alpha$  luminosity are probably underestimated due to flux loss in spectroscopic data. In this study, we examine the halo using deep imaging data taken with the custom narrow-band filter NB906 on Suprime-Cam which enables us for the first time to map out the whole extension of J2329–0301 Ly $\alpha$  halo, and to obtain more accurate measurements on its size and luminosity. We then combine our results with all QSOs' Ly $\alpha$  halo data available in the literature ('compilation sample'), to examine halo properties and their correlations with properties of hosting QSOs over  $z \sim 3 - 6$ . Finally, we discuss the evolution of Ly $\alpha$  halos as a function of QSO age at  $z > 6$ , and as a function of redshift over  $2 < z < 6$ . Because we mainly focus on the properties and evolution of Ly $\alpha$  halos, we do not include QSOs whose halo is undetected in our compilation sample except for  $z > 6$  objects.

The structure of this paper is as follows. We show Suprime-Cam data and its analysis in Section 2, and results on J2329–0301 in Section 3. Results from the compilation sample are shown in Section 4. We discuss the correlations between Ly $\alpha$  halos' scales (luminosity and size) and physical properties of hosting QSOs, and the evolution with QSO age derived from the correlations seen in the  $z > 6$  sample in Section 5.1. We also present discussion on the redshift evolution of Ly $\alpha$  halos and the CGMs from the compilation sample in Section 5.2. Finally, a summary is given in Section 6. Throughout this paper, we use AB magnitudes and adopt a cosmology parameter set of  $(\Omega_m, \Omega_\Lambda, H_0) = (0.3, 0.7, 70 \text{ km s}^{-1} \text{ Mpc}^{-1})$ . In this cosmology, 1 arcsec corresponds to a transverse size of 5.5 pkpc at  $z = 6.4$ .

## 2 DATA AND ANALYSIS

We observed a  $0.219 \text{ deg}^2$  field centered on J2329–0301 with Suprime-Cam (Miyazaki et al. 2002) on the Subaru Telescope through the  $z_r$  and NB906 filters (Goto et al. 2009; Utsumi et al. 2010; Goto et al. 2017). Because details of our observations and data reduction have already been reported (Goto et al. 2009; Utsumi et al. 2010; Goto et al. 2017), we give a brief summary here.

The  $z_r$  band is a special broad-band filter constructed by Shimasaku et al. (2005) with  $\lambda_c = 9853 \text{ \AA}$  and FWHM =  $568 \text{ \AA}$ . The target field was observed with this filter during an engineering run in 2008 August and UH time in 2009 June, together with the  $i'$  and  $z'$  bands. The exposure time was 12,532 sec. As detailed in Goto et al. (2009), the final combined  $z_r$  image has a PSF FWHM of  $0''.62$  and a  $3\sigma$  limiting magnitude of 25.46 mag in a  $1''.2$  aperture (see also Goto et al. 2017).

The NB906 is a custom narrow-band filter developed to investigate the extended Ly $\alpha$  emission of J2329–0301 and Ly $\alpha$  emitters around it (Goto et al. 2017). Its central wavelength and FWHM are  $9050 \text{ \AA}$  and  $158 \text{ \AA}$ , respectively. Willott et al. (2011) and Goto et al. (2012) have shown from their spectroscopic observational data that the J2329–0301’s extended Ly $\alpha$  emission in the CGM spans over  $9000 < \lambda_{\text{obs}} < 9100 \text{ \AA}$ . Our custom narrow-band filter fully covers this wavelength range. We should also mention the fact that different lines can give different systemic redshifts. Recently, a relatively large  $\sim 1000 \text{ km s}^{-1}$  systemic-redshift offset between [C II] and Mg II lines has been reported for some high- $z$  QSOs (e.g., Venemans et al. 2016); we cannot know which is correct. For such QSOs, the dedicated narrow-band filter may fail to catch the Ly $\alpha$  emission if it is designed based on the wrong line. However, since the offset found for J2329–0301 is negligible, [C II] ( $z_{\text{sys}}^{\text{[C II]}} = 6.4164 \pm 0.0008$ ; Willott et al. 2017) and Mg II ( $\lambda_{\text{rest}} = 2799.49 \text{ \AA}$  ( $z_{\text{sys}}^{\text{Mg II}} = 6.417 \pm 0.002$ ; Willott et al. 2010)), the Ly $\alpha$  emission from J2329–0301 is expected to be well within the FWHM of our custom narrow-band filter.

NB906 observations were performed in 2015 September with an exposure time of 23,044 sec. The images were reduced in the same manner as in Utsumi et al. (2010). After subtracting a bias level estimated by an overscan region and flat fielding, we mean-combined all the images into a single mosaic image. Photometric calibration was performed by comparing stars in a reference field 2 deg. away to the north. A photometric transformation equation was determined by convolving Gunn & Stryker (1983)’s stellar SEDs with the response curves that include both optical and atmospheric transmissions. The combined image has a PSF FWHM of  $0''.64$  and a  $5\sigma$  limiting magnitude of 25.73 mag.

We produce a Ly $\alpha$  image in the following two steps. First, we smooth the  $z_r$  and NB906 images with Gaussian kernels to match their PSF sizes to the largest among the raw images before stacking,  $0''.7$  FWHM. Second, we subtract the smoothed  $z_r$  image from the smoothed NB906 image by using the following relation given in the literature (e.g., Yang et al. 2009; Arrigoni Battaia et al. 2016):

$$F_{\text{Ly}\alpha} = F_{\text{NB}} - a \frac{F_{z_r}}{\Delta\lambda_{z_r}} \Delta\lambda_{\text{NB}}, \quad (1)$$

where  $F_{z_r}$  and  $F_{\text{NB}}$  are the fluxes in the  $z_r$  and NB906 bands, and  $F_{\text{Ly}\alpha}$  the flux of the Ly $\alpha$  line;  $\Delta\lambda_{z_r}$  and  $\Delta\lambda_{\text{NB}}$

are the FWHMs of the  $z_r$  and NB906 bands; and  $a$  is a parameter evaluated from the spectral index  $\alpha$ . Because we adopt  $\alpha_\nu = -0.5^1$  (Willott et al. 2007),  $a$  is estimated as 0.96. The SB limit of the Ly $\alpha$  image thus obtained in a  $1''$  aperture is  $6.7 \times 10^{-18} \text{ erg s}^{-1} \text{ cm}^{-2} \text{ arcsec}^{-2}$  at the  $3\sigma$  level. We also stack 100 bright stars in our narrow-band image to produce a PSF image.

### 2.1 The subtraction of the PSF component

To examine whether J2329–0301 has an extended Ly $\alpha$  halo, we remove the contribution from the PSF (i.e., point-source) component of the central QSO. We conduct the PSF subtraction by the following three approaches to find the best way to estimate the halo flux and size.

1) One is to use the PSF image obtained from 100 stars in the NB906 image. First, we scale the PSF image to match the total flux within a  $1''$  radius to that of the Ly $\alpha$  image of J2329–0301. Then, we subtract the scaled PSF image from the J2329–0301 image, and obtain a residual image (*residual image 1*). We confirm that Ly $\alpha$  emission extends over  $\sim 2''$  in radius with  $> 3\sigma$  SB levels. However, there is a hole at the position of J2329–0301 which is probably caused by over-subtraction of the PSF component of the central QSO.

2) The second approach is to use a 2-D Gaussian model in order to minimize the effect of over-subtraction. First, we produce a 2-D Gaussian model image by fitting the PSF image generated from the 100 stars. Then, we scale this Gaussian model image and subtract it from the J2329–0301 image in the same manner as in approach 1). The residual image thus obtained is referred to as *residual image 2*. The presence of extended Ly $\alpha$  emission over  $\sim 1''$  is confirmed also in this image. While a hole is still seen, its size is much smaller than that in *residual image 1*, suggesting that the over-subtracted flux has been largely recovered.

3) The third approach is to use a 2-D Moffat model image. The SB profile and hence the Ly $\alpha$  luminosity of the halo evaluated from *residual image 2* may slightly overestimate the true size and luminosity, because the real PSF profile is known to extend more than a Gaussian profile at large radii albeit with very low amplitudes (e.g., King 1971; Racine 1996; Bernstein 2007). Thus we perform a PSF subtraction with a model Moffat image (Moffat 1969) which can describe well the extended profile of the PSF. The methodology is the same as approach 2). We first make a 2-D Moffat image by fitting the PSF image obtained from the 100 stars. Then we scale the Moffat model image, and subtract it from the J2329–0301 image, which is referred to as *residual image 3*.

We show the results from the above three approaches in Figure 2 (a). At  $1'' < r < 2''$ , the shape and brightness of the SB profiles obtained from the three approaches show a large difference. However, they become consistent within the error bars at  $2'' < r < 4''$ . Because both PSF models (Gaussian and Moffat) reproduce the observed PSF similarly well, we adopt the mean of *residual image 2* and *residual image 3* (produced in approaches 2) and 3)) as better representing the true Ly $\alpha$  emission of the halo, and

<sup>1</sup> Here we define  $f_\nu \propto \nu^{\alpha_\nu}$

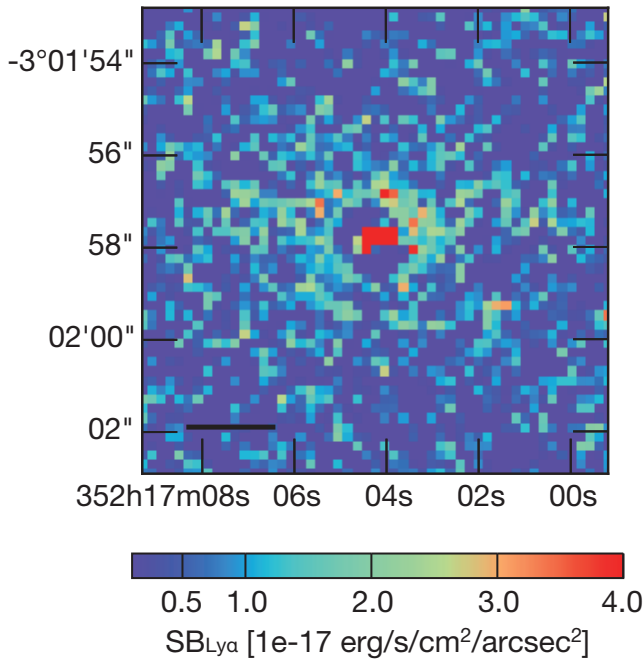


**Figure 1.** The Ly $\alpha$  image of J2329–0301 is presented.

use this image and SB profile in the following analysis. We show the PSF-subtracted Ly $\alpha$  image of J2329–0301 in Figure 1, and the Ly $\alpha$  SB profile of J2329–0301 and the PSF profile in Figure 2 (a). Figure 2 (b) and (c) also compare the tangentially averaged SB profile of J2329–0301’s Ly $\alpha$  halo with those of low- $z$  QSOs and a  $z \sim 6$  QSO obtained by previous studies (Borisova et al. 2016; Farina et al. 2017; Arrigoni Battaia et al. 2019). Note that the SB profile of J2329–0301 is calculated directly from the data.

### 3 RESULTS FROM SUPRIME-CAM DATA

#### 3.1 The luminosity and spatial extent of J2329–0301’s Ly $\alpha$ halo

We find that the Ly $\alpha$  emission of J2329–0301 is more extended than the PSF (Figure 2 (a)) as well as than the continuum emission (Figure 1), thus confirming the presence of a Ly $\alpha$  halo. We use the SB profile (see also Figure 2) to measure the spatial extent of the Ly $\alpha$  halo, i.e., the largest diameter where the SB is above the SB limit, to be  $6''.8$ , or 37 pkpc. The total Ly $\alpha$  luminosity within an annulus of radii from  $1''$  to  $3''.4$  is  $9.8 \pm 2.3 \times 10^{43} \text{ erg s}^{-1}$ . The Ly $\alpha$  luminosity of the QSO is  $6.6 \times 10^{44} \text{ erg s}^{-1}$ .

The Ly $\alpha$  halo of this QSO has also been investigated in previous studies. Goto et al. (2009) have indicated a possible presence of  $4''$ -wide Ly $\alpha$  halo. Spectroscopic follow-up observations by the same group have obtained the total Ly $\alpha$  luminosities of the halo and the hosting QSO to be  $1.7 \times 10^{43} \text{ erg s}^{-1}$  and  $6.2 \times 10^{44} \text{ erg s}^{-1}$ , respectively (Goto et al. 2012). On the basis of spectroscopic data, Willott et al. (2011) have also shown the presence of a Ly $\alpha$  halo over 15 pkpc ( $\sim 2''.7$ ) with a Ly $\alpha$  luminosity of  $8 \times 10^{43} \text{ erg s}^{-1}$ . The Ly $\alpha$  halo found in this study is a factor of  $> 1.7$  more extended, and a factor of  $> 1.9$  more luminous than those obtained by the

previous studies. These discrepancies likely result from differences in the methods to measure halo luminosities. The spectroscopic data could also underestimate the total flux of the halo as well as its extent because of finite slit widths and/or fixed slit directions (Willott et al. 2011; Goto et al. 2012).

#### 3.2 Comparison of the halo SB profile between J2329–0301 and other QSOs

We compare the SB profile of J2329–0301’s halo with those of other QSOs’ in Figure 2 (b) and (c). Black lines represent bright radio-quiet QSOs at  $z \sim 3$  (Borisova et al. 2016) and a blue line is the QSO J0305–3150 at  $z = 6.61$  (Farina et al. 2017); the effect of SB dimming has been corrected for all objects. The profiles of Borisova et al. (2016) QSOs within  $r = 10 \text{ pkpc}$  are plotted as dotted lines.

A comparison with J0305–3150 shows that J2329–0301’s halo has an about 10 times brighter SB profile than J0305–3150’s, albeit with similar profile slopes. As a result, J0305–3150’s halo has a factor 50 fainter total Ly $\alpha$  luminosity and a factor of 4.2 smaller size than J2329–0301’s, despite a deeper SB limit of  $1.1 \times 10^{-18} \text{ erg s}^{-1} \text{ cm}^{-2} \text{ arcsec}^{-2}$  at  $3\sigma$  level (Farina et al. 2017). The SB profile of J2329–0301’s halo lies at the bright end of the distribution of  $z \sim 3$  halos. We estimate the power-law slope of J2329–0301’s SB profile over 10 pkpc to 24 pkpc by fitting the formula  $\text{SB} = C_p r^\alpha$ , where  $C_p$  is a normalization parameter and  $\alpha$  the slope of the power law. We obtain  $(\log_{10}(C_p), \alpha) = (-15.08 \pm 0.47, -1.82 \pm 0.35)$  in physical scales and  $(-13.49 \pm 0.78, -1.82 \pm 0.35)$  in comoving scales. From a survey of  $z = 3$  Ly $\alpha$  halos by the MUSE, Borisova et al. (2016) and Arrigoni Battaia et al. (2019) have reported the power-law slope of the mean SB profile as  $\alpha = -1.8$  and  $-1.96$ , respectively. Although the fitting range of J2329–0301 is narrower than those of the  $z = 3$  Ly $\alpha$  halos, the power-law slope of J2329–0301 is consistent with their measurements. These comparisons suggest that Ly $\alpha$  halos of QSOs can be modeled by profiles with a common shape irrespective of redshift.

We also compare those SB profiles in comoving units by scaling their radii with  $(1+z)$  in Figure 2 (c). First, we find that the difference between J0305–3150 and QSOs from Borisova et al. (2016) seen in Figure 2 (b) is clearly reduced. The SB profile of J0305–3150 comes into overlap with the faint end of Borisova et al. (2016)’s sample, although the SB profile of J2329–0301 is shifted slightly above the bright end. A similarity of SB profiles in comoving units has also been demonstrated by Ginolfi et al. (2018). They have found that the sizes of Ly $\alpha$  halos at  $z \sim 5$  become comparable with those at  $z \sim 3$  when they have accounted for the cosmological growth of dark matter halos by scaling by  $(1+z)$  (Barkana & Loeb 2001). Detailed discussion will be presented in Section 5.2.4.



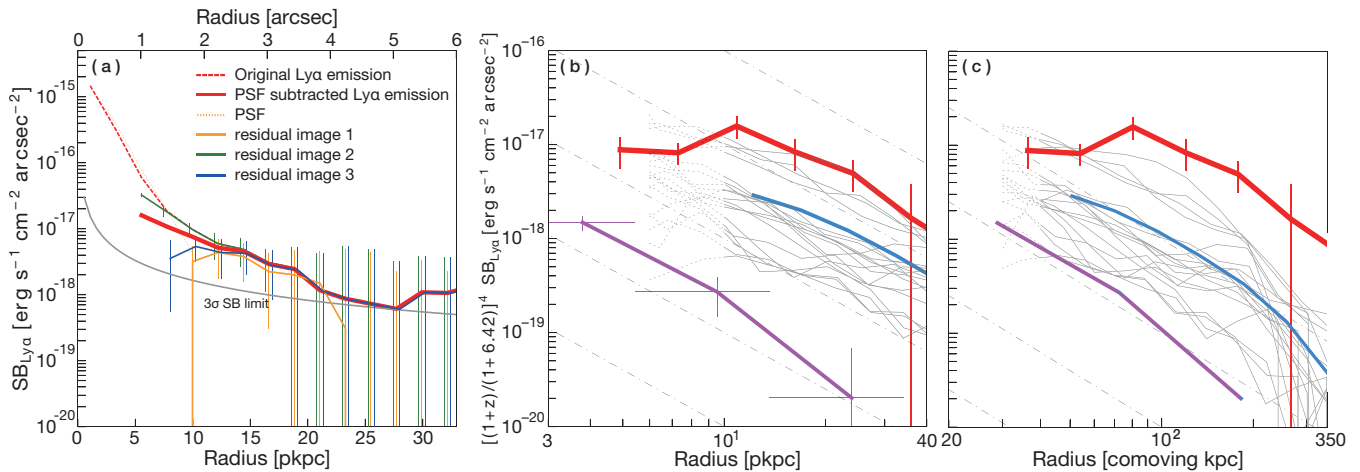


**Figure 2.** (a) Tangentially averaged radial SB profile of the Ly $\alpha$  emission of J2329-0301 together with *residual images*, measured in  $0''.4$  widths. Red dashed and solid lines represent, respectively, the Ly $\alpha$  emission before subtraction of the QSO component and the finally adopted result in this study (i.e., mean of *residual images* 2 and 3). Yellow, green and blue solid lines indicate *residual images* 1, 2, and 3, respectively. The SB profile of the PSF obtained from *NB* data is also plotted with a yellow dotted line. (b) PSF-subtracted, redshift-dimming corrected SB profile of J2329-0301 (red) together with those of radio-quiet QSOs at  $z \sim 3$  (Borisova et al. 2016; black), the mean of the QSO MUSEUM (Arrigoni Battaia et al. 2019; blue) and J0305-3150 at  $z = 6.61$  (Farina et al. 2017; purple). The SB of J2329-0301 is measured up to  $r = 6''.5$  (36 pkpc) in annuli of  $\Delta \log r = 0.17$  pkpc corresponding to  $0''.2 - 2''.2$ . Since Borisova et al. (2016) have regarded only Ly $\alpha$  emission outside of  $r = 10$  pkpc as the halo component, we plot their SB profiles at  $r < 10$  pkpc with dashed lines. The five dash-dotted lines, plotted for reference, are SB( $r$ )  $\propto r^{-2}$  power laws with different amplitudes of  $10^{-14}$ ,  $10^{-15}$ ,  $10^{-16}$ ,  $10^{-17}$ , and  $10^{-18}$  erg s<sup>-1</sup> cm<sup>-2</sup> arcsec<sup>-2</sup> from top to bottom. (c) Same as panel (b) but plotted in comoving scale. (A color figure is available in the online journal.)

#### 4 RESULTS FROM THE COMPILATION SAMPLE: DEPENDENCE OF Ly $\alpha$ HALO PROPERTIES ON REDSHIFT AND QSO PROPERTIES

We plot in Figures 3, 4, and 5 three parameters characterizing Ly $\alpha$  halos (spatial extent  $d$  [pkpc], total Ly $\alpha$  luminosity  $L_{Ly\alpha}$  [erg s<sup>-1</sup>], and the ratio of the halo Ly $\alpha$  luminosity to the hosting QSO's bolometric luminosity  $L_{Ly\alpha}/L_{Bol}$ ) against [1] redshift, [2] two parameters associated with the supermassive black hole of the hosting QSO (black hole mass  $M_{BH}$  [ $M_{\odot}$ ] and the Eddington ratio) and  $L_{Bol}$ , and [3] the dustiness of the hosting QSO (the UV-optical spectral index  $\alpha_{\nu}$ , and the IR-to-UV luminosity ratio  $IRX = L_{IR}/L_{UV}$ ). We have collected all available data from the literature; see footnote.<sup>2</sup> Below we explain each parameter in detail.

<sup>2</sup> Data of QSOs Ly $\alpha$  halos are from Steidel et al. (1991); Heckman et al. (1991a,b); Bremer et al. (1992); Roettgering et al. (1997); van Ojik et al. (1997); Lehnert & Becker (1998); Lehnert et al. (1999); Bergeron et al. (1999); Fynbo et al. (2000); Bunker et al. (2003); Weidinger et al. (2004); Christensen et al. (2006); Francis & McDonnell (2006); Courbin et al. (2008); Barrio et al. (2008); Smith et al. (2009); Yang et al. (2009); Matsuda et al. (2011); North et al. (2012); Decarli et al. (2012); Humphrey et al. (2013); Rauch et al. (2013); Cantalupo et al. (2014); Roche et al. (2014); Martin et al. (2014); Husband et al. (2015); Hennawi et al. (2015); Fumagalli et al. (2016); Borisova et al. (2016); Fathivavsari et al. (2016); North et al. (2017); Bayliss et al. (2017); Kikuta et al. (2017); Farina et al. (2017); Cai et al. (2017, 2018); Ginolfi et al. (2018); Arrigoni Battaia et al. (2019, 2018). Other data of  $M_{BH}$ , Eddington ratio,  $\alpha$ , UV luminosity and FIR or total IR luminosity are

• **Spatial extent  $d$ ,  $d_{org}$ :** We virtually put all objects at  $z = 6.61$  and measure their extents or diameters, at a common SB level of  $1 \times 10^{-18}$  erg s<sup>-1</sup> cm<sup>-2</sup> arcsec<sup>-2</sup> at  $z = 6.61$ .<sup>3</sup> For reference, we also plot original extents taken from the literature with grey-colored symbols in the same panels. In the following sections,  $d$  denotes an anew measured extent and  $d_{org}$  an original one.

• **Total Ly $\alpha$  luminosity  $L_{Ly\alpha}$ :** While an ideal definition of the total luminosity would be the one enclosed within the extent  $d$ , such measurements are available only for a small fraction of the sample. Thus, we use Ly $\alpha$  luminosities presented in the literature. For the two  $z > 6$  QSOs whose halo is undetected (J1030+0524 and J1148+5251, Decarli et al. 2012), we show upper limits derived by assuming a 10 pkpc extent and an average  $5\sigma$  SB value of  $1 \times 10^{-17}$  erg s<sup>-1</sup> cm<sup>-2</sup> arcsec<sup>-2</sup>, following the procedure by Farina et al. (2017).

• **Ratio of the total Ly $\alpha$  luminosity to the hosting QSO' bolometric luminosity,  $L_{Ly\alpha}/L_{Bol}$ :** We define this parameter to characterize the relative prominence of a halo.

•  **$M_{BH}$  and  $L_{Bol}$ :** Black hole masses  $M_{BH}$ , bolometric luminosities  $L_{Bol}$ , and Eddington ratios are taken from the literature if available;  $M_{BH}$  have been estimated us-

from Hughes et al. (1997); Pentericci et al. (2003); Vestergaard (2003); Vestergaard & Osmer (2009); Willott et al. (2007); Shen et al. (2011); Weedman et al. (2012); Calura et al. (2014); Leipski et al. (2014); Pâris et al. (2014, 2017); De Rosa et al. (2014); Ma & Yan (2015); Tsai et al. (2015); Bañados et al. (2016); Murphy & Bernet (2016); Venemans et al. (2016); Kozłowski (2017); Mazzucchelli et al. (2017). We correct both  $L_{Ly\alpha}$  and  $L_{bol}$  based on the adopted cosmology in this study.

<sup>3</sup> It means an SB limit of  $[(1 + 6.61)^4 / (1 + z_{sys})^4] \times 1 \times 10^{-18}$  erg s<sup>-1</sup> cm<sup>-2</sup> arcsec<sup>-2</sup>.

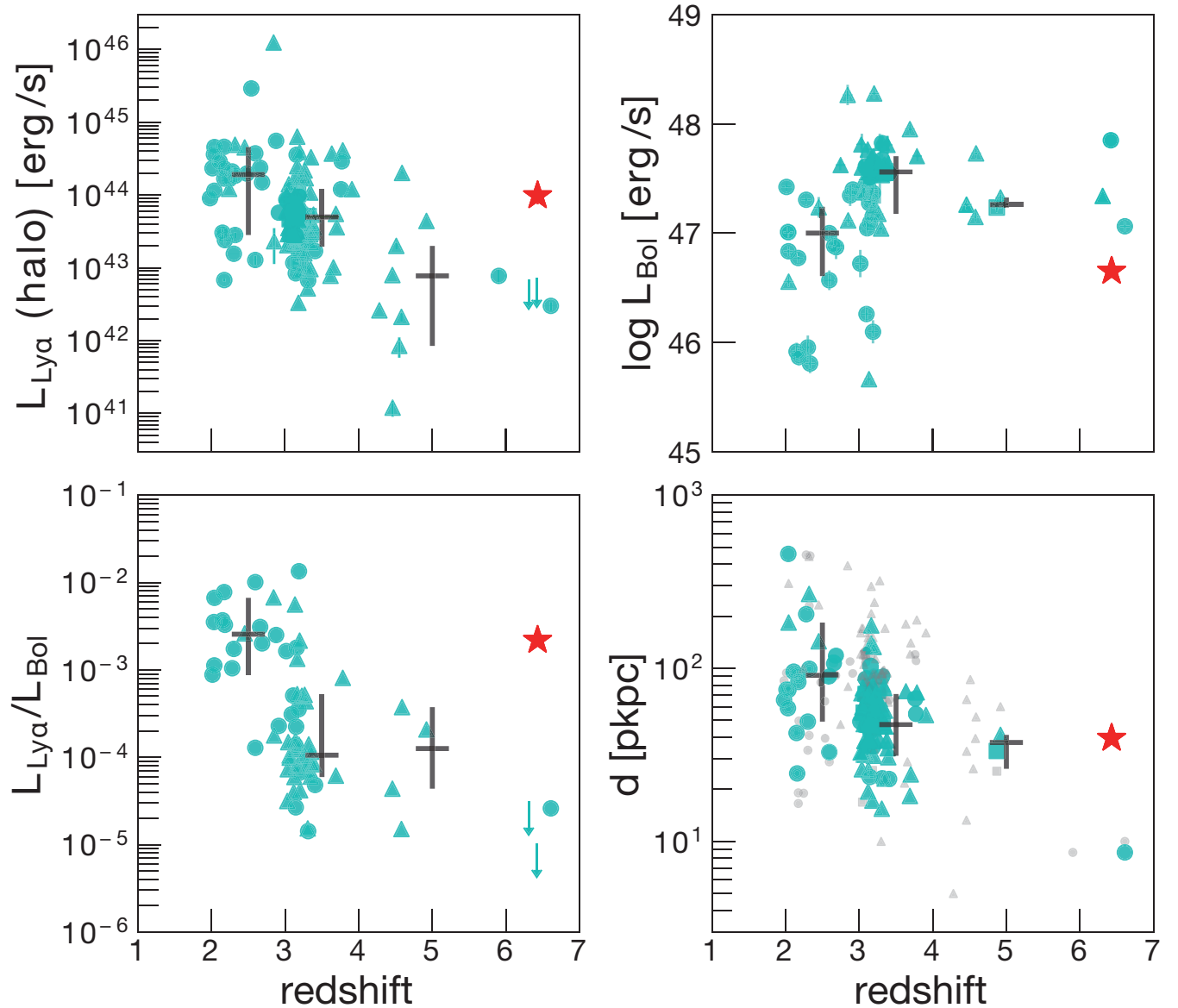


**Figure 3.**  $L_{\text{Ly}\alpha}$  luminosity,  $L_{\text{Bol}}$ ,  $L_{\text{Ly}\alpha}/L_{\text{Bol}}$ , and  $d$ , as a function of redshift. J2329–0301 is plotted in red, while the other QSOs in cyan. Circle and triangle symbols represent radio-loud and radio-quiet QSOs, respectively; those without type information are shown by squares. Median values at  $z = 2, 3$ , and  $4 - 5$  bins are overlaid as black crosses. In the top left and bottom left panels, upper limits of the  $L_{\text{Ly}\alpha}$  luminosity for two undetected  $z > 6$   $\text{Ly}\alpha$  halos are also plotted (Decarli et al. 2012). In the bottom right panel, originally estimated sizes in the literature ( $d_{\text{org}}$ ) are also plotted with grey symbols. (A color figure is available in the online journal.)

ing black hole mass scaling relations with  $\text{Mg II}$ ,  $\text{C IV}$  and  $\text{H}\beta$  luminosities;  $L_{\text{Bol}}$  have been determined from spectral energy distributions (SEDs) from X-ray to radio wavelengths, or from monochromatic luminosities at 5100, 3000, or 1350 Å with bolometric corrections (Richards et al. 2006; Shen et al. 2008).

- **Spectral index  $\alpha_\nu$ :** Taken from the literature if available. They have been derived by fitting a single power law of  $f_\nu \propto \nu^{\alpha_\nu}$  over 1000–3000 or 1000–10000 Å in the rest-frame (Pentericci et al. 2003; Willott et al. 2007; Leipski et al. 2014; Pâris et al. 2014, 2017; Mazzucchelli et al. 2017).

- **IR to UV luminosity ratio, IRX:** This ratio, called the IR excess, is an indicator of the dustiness of a galaxy.

We estimate IRX values with UV luminosities derived from absolute magnitudes at 1450 or 1550 Å and total IR luminosities given in the literature. If a total IR luminosity is unavailable, a total far-IR luminosity is used instead. Due to few radio studies in our compilation sample, the number of objects with IRX estimates is limited.

Unfortunately, not all objects have a full set of measurements except for  $d_{\text{org}}$  and redshift. For this reason, different subsamples are used in different plots, as summarized in Table 1. Also shown in this table is Spearman’s rank correlation coefficient  $\rho$  for each plot in Figures 4 and 5. The standard deviation of  $\rho$  obtained from 1000 times data resampling is considered as its error.

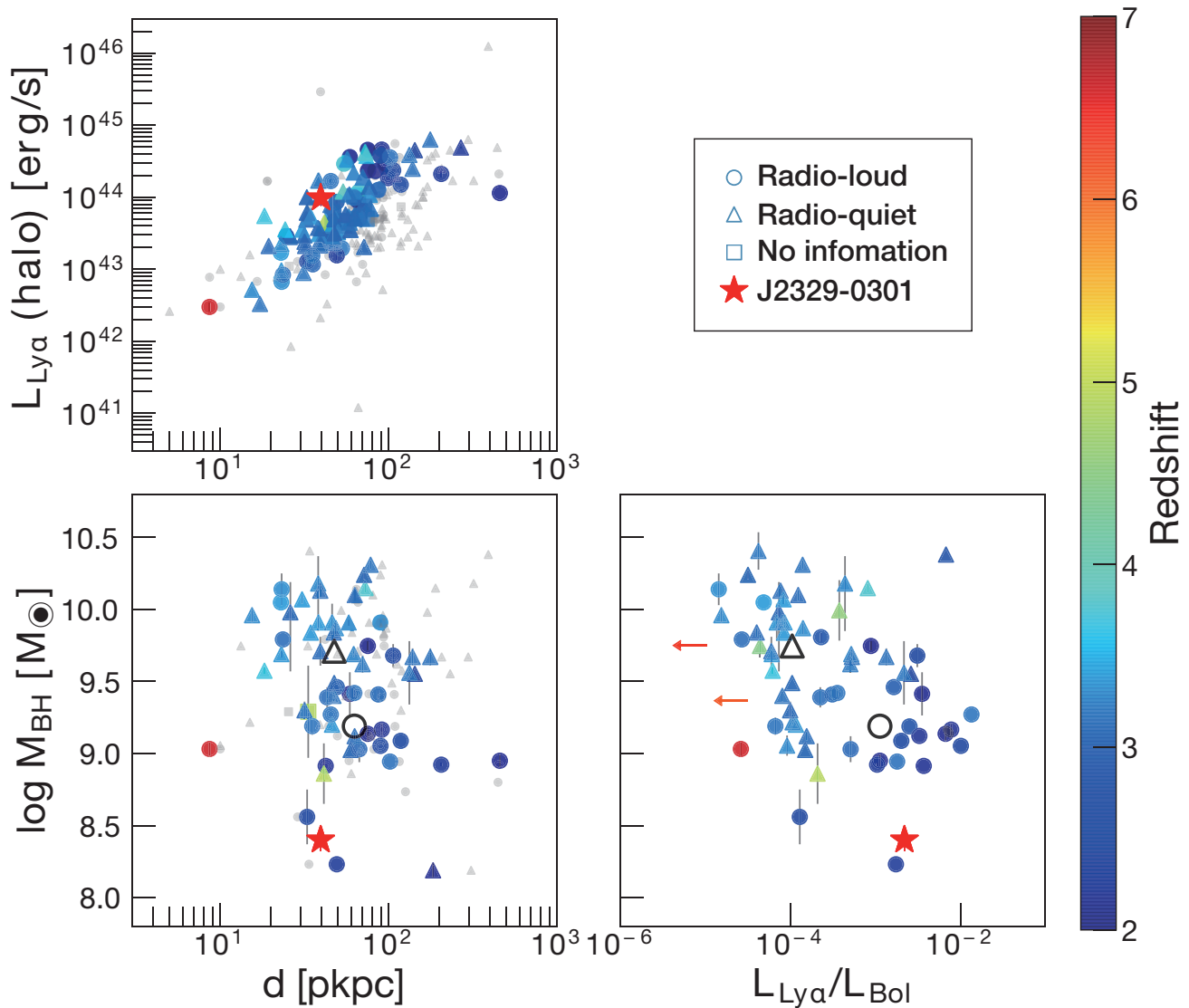


**Figure 4.** Correlations of  $d$  and  $L_{\text{Ly}\alpha}/L_{\text{Bol}}$  with the  $L_{\text{Ly}\alpha}$  and  $M_{\text{BH}}$  of hosting QSOs. J2329–0301 is shown as a star. Circle and triangle symbols represent radio-loud and radio-quiet QSOs, respectively; those without information are shown by squares. All symbols except grey ones are color-coded according to redshift. The  $L_{\text{Ly}\alpha}/L_{\text{Bol}}$  of J1030+0524 and J1148+5251 from Decarli et al. (2012) is an upper limit. (Left)  $L_{\text{Ly}\alpha}$  and  $M_{\text{BH}}$  as a function of  $d$ . Original  $d$  estimates taken from the literature are also plotted with grey symbols. (Right)  $M_{\text{BH}}$  plotted against  $L_{\text{Ly}\alpha}/L_{\text{Bol}}$ . (Bottom) Median values of the radio-loud and quiet samples are also displayed by a void circle and a void triangle. (A color figure is available in the online journal.)

#### 4.1 Redshift dependence of halo properties

Figure 3 shows the  $L_{\text{Ly}\alpha}$ ,  $L_{\text{Bol}}$ ,  $L_{\text{Ly}\alpha}/L_{\text{Bol}}$  and  $d$  of Ly $\alpha$  halos as a function of redshift. The median values at  $z = 2, 3$ , and  $4 - 5$  are also plotted with an error bar for reference. We find a gradual decline in  $L_{\text{Ly}\alpha}$ ,  $L_{\text{Ly}\alpha}/L_{\text{Bol}}$  and  $d$  with redshift, while  $L_{\text{Bol}}$  does not show such a decline. In addition, the decrease in the spatial extent is notable, which is found in both  $d$  and  $d_{\text{org}}$ . Interestingly, J2329–0301’s halo has an spatial extent as small as average  $z \sim 2 - 3$  halos despite having relatively high  $L_{\text{Bol}}$  and  $L_{\text{Ly}\alpha}/L_{\text{Bol}}$  values.

The observed declines of  $L_{\text{Ly}\alpha}$ ,  $L_{\text{Ly}\alpha}/L_{\text{Bol}}$  and  $d$  with redshift may be partly artificial. Different kinds of observations (imaging or spectroscopy), different SB limits,

and different target selections among the studies may induce artificial trends. In fact, some previous studies have found similar declines of  $d_{\text{org}}$  and/or  $L_{\text{Ly}\alpha}$  with redshift (Farina et al. 2017; Ginolfi et al. 2018), whereas others have not (Fathivavsari et al. 2016). Nevertheless, Figure 3 clearly demonstrates a systematic trend that bright ( $> \text{several} \times 10^{44} \text{ erg s}^{-1}$ ) and extended ( $> 100 \text{ pkpc}$ ) Ly $\alpha$  halos are absent at  $z > 4$ . Considering the facts that the average  $L_{\text{Bol}}$  is unchanged or even increases with redshift, and that the bolometric luminosity is proportional to the ionizing luminosity in the first order (e.g., Lu & Yu 1999), bright and extended Ly $\alpha$  halos such as found in  $z = 2 - 3$  (e.g., Cantalupo et al. 2014; Martin et al. 2014;

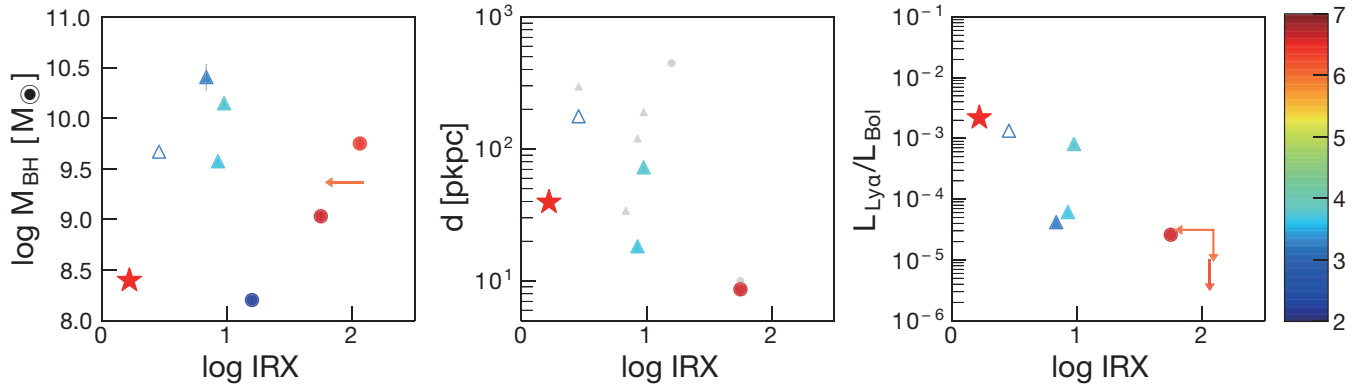


**Figure 5.** Correlations of IRX with  $M_{\text{BH}}$ ,  $d$  and  $L_{\text{Ly}\alpha}/L_{\text{Bol}}$ . The meanings of symbols and colors are the same as in Figure 4. The IRX value of a QSO shown by a white triangle is derived using a FIR luminosity instead of a total IR luminosity. (A color figure is available in the online journal.)

**Table 1.** The parameters and the number of objects plotted in individual figures.

Figure number	$N_{\text{sample}}$	Spearman's $\rho$
Figure 3 $L_{\text{Ly}\alpha}$ vs redshift	135	–
Figure 3 $L_{\text{Bol}}$ vs redshift	78	–
Figure 3 $L_{\text{Ly}\alpha}/L_{\text{Bol}}$ vs redshift	71	–
Figure 3 $d$ vs redshift cyan points	109 (144)	– –
Figure 4 $L_{\text{Ly}\alpha}$ vs $d$ painted points	106 (133)	$0.75 \pm 0.05$ ( $0.57 \pm 0.07$ )
Figure 4 $M_{\text{BH}}$ vs $d$ painted points	59 (72)	$-0.28 \pm 0.13$ ( $-0.16 \pm 0.13$ )
Figure 4 $M_{\text{BH}}$ vs $L_{\text{Ly}\alpha}/L_{\text{Bol}}$	65	$-0.44 \pm 0.11$
Figure 5 $M_{\text{BH}}$ vs IRX	9	$0.12 \pm 0.43$
Figure 5 $d$ vs IRX	5 (7)	$-0.50 \pm 0.52$ ( $-0.04 \pm 0.52$ )
Figure 5 $L_{\text{Ly}\alpha}/L_{\text{Bol}}$ vs IRX	8	$-0.54 \pm 0.43$
Figure 6 $\text{SB}_{\text{Ly}\alpha}^{r=10}$ vs $z$	124	–

The number in parentheses in  $N_{\text{sample}}$  column is the number of objects with  $d_{\text{org}}$  measurements. The standard deviation of Spearman's  $\rho$  derived from 1000 times resampling is regarded as the error in the  $\rho$  estimate.

Hennawi et al. 2015; Borisova et al. 2016; Cai et al. 2017; Arrigoni Battaia et al. 2018) should be detected even at  $z > 4$  if there is no evolution. This striking result indicates some redshift evolution of Ly $\alpha$  halos. We will discuss this matter in Section 5.2.3.

#### 4.2 Correlations with properties of hosting QSOs

We find no significant correlation between halo properties and QSOs'  $L_{\text{Ly}\alpha}$ ,  $L_{\text{Ly}\alpha}/L_{\text{Bol}}$ ,  $M_{\text{BH}}$  and Eddington ratio except in  $d$  vs  $L_{\text{Ly}\alpha}$ . Thus, we only display  $d$  vs  $L_{\text{Ly}\alpha}$  and two plots showing very weak correlations in Figure 4.

A positive and strong correlation is seen between  $d$  and  $L_{\text{Ly}\alpha}$  (top left plot of Figure 4), with a Spearman's coefficient of  $\rho = 0.75 \pm 0.05$  ( $0.57 \pm 0.07$ ) if  $d_{\text{org}}$  is used instead.<sup>4</sup> In fact, such a positive correlation is naturally expected from the finding in Section 3.2 that Ly $\alpha$  halos have similar SB profiles. We derive the best-fit linear regressions in the log-log plot of  $\log L_{\text{Ly}\alpha} [\text{erg s}^{-1}] = (41.53 \pm 0.11) + (1.32 \pm 0.06) \times \log d [\text{kpc}]$  and  $\log L_{\text{Ly}\alpha} = (43.79 \pm 0.21) + (0.25 \pm 0.12) \times \log d_{\text{org}}$ . A similar correlation has also been reported in the literature (Fathivavsari et al. 2016; North et al. 2017). Fathivavsari et al. (2016) have found the best-fit power law of the form  $d_{\text{org}} \propto L_{\text{Ly}\alpha}^b$  with  $b = 0.5$  for Christensen et al. (2006)'s sample and  $b = 0.7$  for their own sample, corresponding to a slope of 2 and 1.42 in the  $L_{\text{Ly}\alpha}$  vs  $\log d_{\text{org}}$  plot.

No apparent correlation is found between  $d$  and  $M_{\text{BH}}$  with Spearman's  $\rho$  of  $\rho = -0.28 \pm 0.13$  ( $\rho = -0.16 \pm 0.13$  for  $d_{\text{org}}$ ), while a moderate correlation is seen between  $L_{\text{Ly}\alpha}/L_{\text{Bol}}$  and  $M_{\text{BH}}$  with  $\rho = 0.44 \pm 0.11$  (bottom two panels in Figure 4). If limited to the  $z > 6$  QSOs colored in red, we find a possible negative trend in both panels, despite a very small sample size, that QSOs with a larger  $M_{\text{BH}}$  tend to possess a larger and brighter Ly $\alpha$  halo. If larger  $M_{\text{BH}}$  means a longer elapsed time, the weak decrease in  $L_{\text{Ly}\alpha}/L_{\text{Bol}}$  with  $M_{\text{BH}}$  found among the  $z > 6$  QSOs may indicate that younger QSOs possess more luminous (and possibly more extended; lower left panel of Figure 4) Ly $\alpha$  halos. We discuss this matter in Section 5.1.

The  $L_{\text{Ly}\alpha}/L_{\text{Bol}}$  vs  $M_{\text{BH}}$  distribution also shows another tendency depending on radio loudness. We display the median values of  $L_{\text{Ly}\alpha}/L_{\text{Bol}}$  and  $M_{\text{BH}}$  for the radio-loud and quiet samples with void circle and triangle symbols, respectively, in the bottom two panels of Figure 4. Radio-loud QSOs are found to have more luminous Ly $\alpha$  halos. This may be due to radio jets associated with radio-loud QSOs, which make it easy for ionizing photons to escape out to the CGM.

<sup>4</sup> We regard the standard deviation of Spearman's rank correlation  $\rho$  obtained from 1000 times resampling of data points as  $1\sigma$  error.



### 4.3 $M_{\text{BH}}$ , $d$ and $L_{\text{Ly}\alpha}/L_{\text{Bol}}$ vs the dustiness of QSOs

Finally, we examine the correlations of  $M_{\text{BH}}$ ,  $d$  and  $L_{\text{Ly}\alpha}/L_{\text{Bol}}$  with  $\alpha_{\nu}$  and IRX. The spectral index  $\alpha_{\nu}$  is the power-law index of spectra, with larger values meaning bluer spectra. The IRX is an indicator of dustiness, with higher values meaning higher dust obscuration.

We do not find any significant correlation with  $\alpha_{\nu}$ , with small Spearman's  $\rho$  of 0.32, 0.05 and  $-0.23$  for  $M_{\text{BH}}$ ,  $d$  and  $L_{\text{Ly}\alpha}/L_{\text{Bol}}$ . On the other hand, moderate negative correlations are indicated in the plots of  $d$  and  $L_{\text{Ly}\alpha}/L_{\text{Bol}}$  against IRX with  $\rho = (0.12 \pm 0.43, -0.50 \pm 0.52, -0.54 \pm 0.43)$  for  $(M_{\text{BH}}, d, L_{\text{Ly}\alpha}/L_{\text{Bol}})$ , although the errors are large due to small sample sizes (Figure 5). Similarly, the QSOs at  $z > 6$  colored in red appear to have a trend that those with larger IRX values possess more massive black holes but smaller halo sizes and fainter halo luminosities. We discuss implications of these trends in Section 5.1.

## 5 DISCUSSION

### 5.1 Coevolution of QSOs and their Ly $\alpha$ halos

#### 5.1.1 Correlation between Ly $\alpha$ halo properties and the dustiness of QSOs at $z > 6$

Among the four  $z > 6$  QSOs with Ly $\alpha$  halo data, only J2329–0301 has a distinguishing Ly $\alpha$  halo. In this subsection, we discuss what makes this difference by examining the physical properties of the four  $z > 6$  QSOs presented in Table 2 with help of the results obtained in Section 4.3.

We find from Table 2 that J2329–0301 has the lowest IR luminosity and the lowest dust mass among the four, while the other three QSOs are luminous in IR or possessing a large amount of dust, implying a close relation between Ly $\alpha$  halos and the amount of dust. We also find in Section 4.3 that less dusty QSOs with larger  $\alpha$  and/or smaller IRX values tend to have more extended and bright Ly $\alpha$  halos. The relation between dust content and the presence of Ly $\alpha$  halos has also been discussed in the literature. Although not for QSOs but LAEs, Hayes et al. (2013) have found an anti-correlation between the relative extent of the Ly $\alpha$  halo to the star-forming disk and indicators of dust content, indicating that a low dust content is required to produce an extended Ly $\alpha$  halo. Moreover, Willott et al. (2011, 2013) have attributed the significant Ly $\alpha$  halo of J2329–0301 to the non-detection of dust continuum emission, because the Ly $\alpha$  halo of J2329–0301 could be generated by ionizing photons that easily escape to the CGM due to a small dust content. According to their arguments, J2329–0301 is in a rare phase that the QSO feedback effectively shuts down the star formation activity of the host galaxy, resulting in a small dust content. Our findings from Table 2 and Section 4.3 support these suggestions, although based on only four objects. Therefore, the amount of dust probably determines the presence or absence of a Ly $\alpha$  halo.

We also notice that the other parameters of J2329–0301 ( $M_{\text{BH}}$ ,  $L_{\text{Bol}}$  and star-formation rate SFR) are also lower than those of the remaining three QSOs (see Table 2). Additionally, we find that all parameters but the Eddington ratio ( $L_{\text{Bol}}$ , SFR, IR luminosity, dust mass) increase with  $M_{\text{BH}}$

from J2329–0301 through J0305–3150 and J1030+0524 to J1148+5251. If a larger  $M_{\text{BH}}$  means a longer elapsed time, the increase in these physical parameters with  $M_{\text{BH}}$  may naively indicate their evolution. A bright Ly $\alpha$  halo may appear only in an early phase of black hole growth.

A black hole evolves with its host galaxy, that is so called co-evolution (e.g., Magorrian et al. 1998; Merritt & Ferrarese 2001; McLure & Dunlop 2002; Marconi & Hunt 2003; Graham & Scott 2013; Kormendy & Ho 2013 and reference therein). According to the theoretical framework of galaxy evolution (e.g., Hopkins et al. 2008), the accretion disk around a black hole becomes visible in the rest-UV to optical wavelengths (and observed as a QSO) when the dust surrounding it is destroyed or blown away by negative feedbacks. After that, the QSO actively radiates UV emission with a high Eddington ratio. We call the phase when the QSO has just started to shine in UV the *young QSO phase*. Then the QSO is supposed to evolve by increasing its stellar mass and dust mass, as well as black hole mass, by acquiring gas from the IGM (*mature QSO phase*). Finally, the QSO's activity will weaken because the gas is consumed and dispersed (*old QSO phase*). In this scenario, an extended and bright Ly $\alpha$  halo exists only in the *young QSO phase* where a large amount of ionizing photons from the QSO easily escape to the circum-galactic region without strong dust extinction, and ionize neutral hydrogen of the CGM. In the *mature* and *old phases*, on the other hand, an enormous amount of dust in the inter-stellar medium (ISM) makes ionizing photons difficult to leak away, thus preventing the CGM, even if it exists, from radiating Ly $\alpha$  emission. Thus, both the presence of a Ly $\alpha$  halo and the trends seen in the physical parameters of the four  $z > 6$  QSOs can be consistently interpreted in the evolutionary framework of QSOs. J2329–0301 with a distinguishing Ly $\alpha$  halo owing to a small amount of dust is probably in the *young QSO phase*, while the other three with massive black holes ( $M_{\text{BH}} > 10^9 M_{\odot}$ ) and high dust masses ( $M_{\text{dust}} > 10^8 M_{\odot}$ ) are likely in the *mature* or *old QSO phase*.

Although we find a negative trend that the luminosity and size of Ly $\alpha$  halos decrease with dustiness and  $M_{\text{BH}}$  among four  $z > 6$  QSOs, this may happen by chance. In order to confirm the presence of this trend, observations of Ly $\alpha$  emission targeting  $z > 6$  QSOs with dustiness and  $M_{\text{BH}}$  estimates are needed.

#### 5.1.2 Physical properties of QSOs and their Ly $\alpha$ halos at low- $z$

We discuss the relation between Ly $\alpha$  halo properties and QSO properties at  $z \sim 2 - 3$ . In Section 4.3, we find that there are possible weak tendencies especially between Ly $\alpha$  halo scales ( $d$  and  $L_{\text{Ly}\alpha}/L_{\text{Bol}}$ ) and the IRX, although Spearman's  $\rho$  values have large error bars due to a small sample size. This trend is comparable with the one seen for the  $z > 6$  QSOs over a wider IRX range. It may imply that dust abundance is also key to producing a Ly $\alpha$  halo around low- $z$  QSOs. However, again, this possible negative trend may be statistically insignificant because it is based on only several QSOs. Thus we need more measurements of both IRX and Ly $\alpha$  halo scales to low- $z$  QSOs. Fortunately, Ly $\alpha$  halos have already been detected for dozens of QSOs at  $z \sim 3$  in

**Table 2.** Physical parameters of QSOs at  $z > 6$ 

	J2329–0301	J0305–3150	J1030+0524	J1148+5251
Ly $\alpha$ halo	detection	detection	non-detection	non-detection
$\log M_{\text{BH}} [M_{\odot}]$	8.40	8.98 – 9.08	9.00 – 9.56	9.75
$\log L_{\text{Bol}} [\text{erg s}^{-1}]$	46.60	47.06	47.37	47.85
Eddington ratio	1.3	0.68 – 0.74	0.50	1.01
SFR [ $M_{\odot} \text{ yr}^{-1}$ ]	13	545	< 3165	3801 – 6000
$\log L_{\text{IR}} [L_{\odot}]$	10.95	12.83	< 13.53	13.74
$\log M_{\text{dust}} [M_{\odot}]$	< 7.00	8.65 – 9.38	< 8.63	8.85
References	1, 2, 3, 4	5, 6	4, 6, 7, 8, 9	4, 8, 9, 10

Note. References are (1) Willott et al. 2010, (2) Willott et al. 2017, (3) Decarli et al. 2018, (4) Calura et al. 2014, (5) De Rosa et al. 2014, (6) Venemans et al. 2016, (7) Jiang et al. 2007, (8) Jiang et al. 2006, (9) Lyu et al. 2016, and (10) Leipski et al. 2014.

the literature (Borisova et al. 2016; Arrigoni Battaia et al. 2019). IR or radio data of these QSOs would provide IRX values, and evaluate the correlation between dustiness and Ly $\alpha$  halo scales.

We also find that some low- $z$  QSOs with massive black holes ( $M_{\text{BH}} > 10^9 M_{\odot}$ ) have relatively large,  $d < 100$  pkpc, Ly $\alpha$  halos (see Figure 4), whereas none of the  $z > 6$  QSOs with the same mass range has such a halo, despite the fact that all the QSOs have similar trends in  $d$  vs IRX and  $L_{\text{Ly}\alpha}/L_{\text{Bol}}$  vs IRX. Therefore, we infer that the discrepancy of the presence/absence of Ly $\alpha$  halos at  $M_{\text{BH}} > 10^9 M_{\odot}$  is due to differences in the evolutionary track, and/or differences in physical properties of the ISM, such as dust density, gas mass/density, and the size of the star-forming disk.

In Sections 5.1.1 and above, we have found possible negative correlations of Ly $\alpha$  luminosity with  $M_{\text{BH}}$  or IRX, and proposed a hypothesis that QSOs in younger phase have larger Ly $\alpha$  halos. Note, however, that the following two possibilities cannot be ruled out. First is that the observed correlations have arisen just by chance due to small samples. In particular, the  $z > 6$  sample consists of only four objects among which two have only an upper limit of  $L_{\text{Ly}\alpha}$ . The second possibility is that the two negative correlations are real but they are caused by other physics which we do not consider, because dust abundance is not the only factor to determine the size and luminosity of an extended Ly $\alpha$  halo. If dust has a clumpy distribution, ionizing photons can escape from the host galaxy more easily, making a large and bright Ly $\alpha$  halo. It has also been suggested that a wider opening angle gives a high escape fraction of ionizing photons (e.g. Trainor & Steidel 2013; but see also Hennawi & Prochaska 2013). The resonant scattering of Ly $\alpha$  photons by H I gas (if any) in the CGM can also contribute to extended halos, where the escape fraction of Ly $\alpha$  photons is determined by the H I gas distribution and dynamics as well as the dust distribution in the inter-stellar medium (ISM) (e.g. Laursen & Sommer-Larsen 2007; Laursen et al. 2009; Dijkstra & Kramer 2012; Verhamme et al. 2012; Yajima et al. 2018). It may not be easy to reproduce the observed correlations with these physical factors, because one has to assume, for example, that opening angle is dependent on  $M_{\text{BH}}$  and IRX. However, the current data cannot

rule out such dependencies. We will leave further discussion of this issue for future work.

## 5.2 The CGM around QSOs

### 5.2.1 Is the CGM of J2329–0301 optically thin or thick?

Hennawi & Prochaska (2013) have proposed several models which can explain the observed SB and Ly $\alpha$  luminosity of Ly $\alpha$  halos around QSOs by assuming different origins of Ly $\alpha$  emission. Because QSOs' Ly $\alpha$  halos are known to be mainly due to fluorescence (e.g., Hogan & Weymann 1987; Rees 1988; Gould & Weinberg 1996; Haiman & Rees 2001; Alam & Miralda-Escudé 2002; Cantalupo et al. 2005; Kollmeier et al. 2010), here we consider their fluorescence model. Here we examine the optical thickness of J2329–0301's halo by following the same approach as in Farina et al. (2017). First, we test the case that J2329–0301 is surrounded by optically thick gas. In this scenario, Ly $\alpha$  emission produced through recombination is mainly from the skin of clouds, and can be quantified with

$$\frac{L_{\text{Ly}\alpha}}{10^{44} \text{ erg s}^{-1}} = 7.8 \times f_c^{\text{thick}} \frac{L_{\nu\text{LL}}}{10^{30} \text{ erg s}^{-1} \text{ Hz}^{-1}}, \quad (2)$$

where  $L_{\text{Ly}\alpha}$  is the total Ly $\alpha$  luminosity of the halo,  $f_c^{\text{thick}}$  the covering factor for optically thick clouds, and  $L_{\nu\text{LL}}$  the ionizing luminosity evaluated at the Lyman limit (Hennawi & Prochaska 2013; Farina et al. 2017). Then, the  $L_{\text{Ly}\alpha}$  above which the CGM is in the optically thick regime is derived as  $L_{\text{Ly}\alpha} = 3.1 \times 10^{44} \text{ erg s}^{-1}$  by using the ionizing luminosity<sup>5</sup>  $L_{\nu\text{LL}} = 4.0 \times 10^{30} \text{ erg s}^{-1} \text{ Hz}^{-1}$ , and  $f_c^{\text{thick}} = 0.1$  as has been obtained for small-scale Ly $\alpha$  emission found around  $z = 2 - 3$  QSOs (Hennawi & Prochaska 2013). This  $L_{\text{Ly}\alpha}$  value is about a factor of three larger than the observed value,  $L_{\text{Ly}\alpha} = 9.8 \times 10^{43} \text{ erg s}^{-1}$ . Thus, in order for J2329–0301's Ly $\alpha$  halo to be optically thick,  $f_c^{\text{thick}}$  must be relatively low, below the observed value of 0.03. However, optically thick gas around QSOs is reported to have higher  $f_c^{\text{thick}}$  values of  $f_c^{\text{thick}} > 0.2$  by an independent

<sup>5</sup> The  $L_{\nu\text{LL}}$  is derived using the relations found from QSOs stacked spectra in Lusso et al. (2015) with the 1450 Å absolute magnitude of J2329–0301  $M_{1450} = -25.25$ .

method (Prochaska et al. 2013b). Therefore, optically thick gas is not probably the case. We should, however, note that optically thick gas with an unusually small covering fraction cannot be ruled out.

Next, we consider the case that the CGM is optically thin. If a QSO is surrounded by optically thin gas, it would be sufficiently ionized by ionizing photons from the QSO. Gas of a Ly $\alpha$  halo is considered to be optically thin if the neutral column density averaged over the halo  $\langle N_{\text{H I}} \rangle$  is less than  $10^{17.2} \text{ cm}^{-2}$  (Hennawi & Prochaska 2013). We evaluate  $\langle N_{\text{H I}} \rangle$  of J2329–0301’s halo. According to Hennawi & Prochaska (2013),  $\langle N_{\text{H I}} \rangle$  is expressed by

$$\frac{\langle N_{\text{H I}} \rangle}{10^{17.2} \text{ cm}^{-2}} = 1.1 \left( \frac{L_{\text{Ly}\alpha}}{10^{44} \text{ erg s}^{-1}} \right) \left( \frac{L_{\nu\text{LL}}}{10^{30} \text{ erg s}^{-1} \text{ Hz}^{-1}} \right)^{-1}. \quad (3)$$

We obtain  $\langle N_{\text{H I}} \rangle = 10^{16.6} \text{ cm}^{-2}$ , which is a factor of 3.7 lower than the threshold value. Again, J2329–0301 requires a very small  $f_c^{\text{thick}}$  value of  $< 0.03$  to regard its CGM as optically thick, that is inconsistent with  $f_c^{\text{thick}}$  found around low- $z$  QSOs (Prochaska et al. 2013b). Therefore, these two tests indicate that the optically thin CGM is probably the case for J2329–0301.

### 5.2.2 Is the CGM of the other QSOs optically thin or thick?

We also use Equation 3 to evaluate  $\langle N_{\text{H I}} \rangle$  for the other QSOs in the compilation sample. Because not all objects have  $L_{\nu\text{LL}}$  measurements, we evaluate  $L_{\nu\text{LL}}$  by scaling the value of J2329–0301 by the  $L_{\text{Bol}}$  ratio between the object in question and J2329–0301 assuming that  $L_{\nu\text{LL}}$  is proportional to  $L_{\text{Bol}}$ . Among the objects in the compilation sample, 47% (68 QSOs) have both  $L_{\text{Bol}}$  and  $L_{\text{Ly}\alpha}$  measurements, and we find almost all of them to be optically thin. For those without  $L_{\text{Bol}}$  measurements but with  $L_{\text{Ly}\alpha}$  data (44% or 64 objects of the compilation sample), we just use the  $L_{\nu\text{LL}}$  of J2329–0301, and again find that almost all are optically thin. If an object is fainter in  $L_{\nu\text{LL}}$  but brighter in  $L_{\text{Ly}\alpha}$  than J2329–0301, its CGM would be regarded as optically thick. However, the fraction of such objects is likely to be less than 31%; 45 objects are more luminous in  $L_{\text{Ly}\alpha}$  than J2329–0301 and only 2 have higher  $L_{\text{Ly}\alpha}$  and lower  $L_{\text{Bol}}$  than J2329–0301. We cannot evaluate  $\langle N_{\text{H I}} \rangle$  for the remaining 8% of the compilation sample which have neither  $L_{\text{Ly}\alpha}$  or  $L_{\text{Bol}}$ . To summarize, at least 88% of the compilation sample are probably optically thin.

### 5.2.3 Possible redshift evolution of the CGM

We find that  $L_{\text{Ly}\alpha}$ ,  $L_{\text{Ly}\alpha}/L_{\text{Bol}}$  and  $d$  of Ly $\alpha$  halos decrease with redshift. As described in Section 4.1, these decreasing trends seem to be real because no QSO at  $z > 4$  has an extended Ly $\alpha$  halo despite having similarly bright  $L_{\text{Bol}}$  to lower- $z$  objects. Furthermore, the amplitude of the SB profile appears to decrease with redshift as shown in Figure 2 (b) except that of J2329–0301 (Borisova et al. 2016; Farina et al. 2017). The redshift evolution of  $L_{\text{Ly}\alpha}$ , spatial extent and SB amplitude has also been discussed in the literature (North et al. 2012; Farina et al. 2017; Ginolfi et al. 2018). These pieces of evidence together with our finding

that there is no bright and extended Ly $\alpha$  halos at  $z > 4$  appear to indicate some evolution of the CGM.

In order to obtain further insights, we compare the characteristic SB profile of Ly $\alpha$  halos among three redshift bins of  $2 < z < 3$ ,  $3 < z < 4$ , and  $4 < z < 6$  that denote  $z = 2$ , 3, and 4–5. The SB profiles of  $z > 6$  QSOs are discussed separately because of a very small sample size. Since not all objects in the compilation sample have SB data, we derive the characteristic SB profile at each redshift bin in the following manner.

i) For each object, we calculate the SB at 10 pkpc radius ( $\text{SB}_{\text{Ly}\alpha}^{r=10}$ ) from  $L_{\text{Ly}\alpha}$  and  $d_{\text{org}}$ . We choose 10 pkpc radius, since it is large enough to be within halos, being close to their inner most radii (e.g., Borisova et al. 2016), and small enough to have high- $S/N$  Ly $\alpha$  emission. Because of this definition for deriving  $\text{SB}_{\text{Ly}\alpha}^{r=10}$ , we only use objects with  $d_{\text{org}} \geq 20$  pkpc (see also Table 1).  $\text{SB}_{\text{Ly}\alpha}^{r=10}$  values after correction for SB dimming are shown in Figure 6 (left).

ii) We then use  $\text{SB}_{\text{Ly}\alpha}^{r=10}$  values to calculate the median  $\text{SB}_{\text{Ly}\alpha}^{r=10}$  for each redshift bin (blue, cyan and green crosses in Figure 6 left). Because  $\text{SB}_{\text{Ly}\alpha}^{r=10}$  values are widely distributed from  $10^{-21}$  to  $10^{-15} \text{ erg s}^{-1} \text{ cm}^{-2} \text{ arcsec}^{-2}$ , we adopt not an average but a median for the characteristic SB, which is found to be  $\langle \text{SB}_{\text{Ly}\alpha}^{r=10} \rangle = (1.4 \times 10^{-17}, 3.6 \times 10^{-18}, 8.7 \times 10^{-19}) \text{ erg s}^{-1} \text{ cm}^{-2} \text{ arcsec}^{-2}$  for  $z = (2, 3, 4-5)$ .

iii) Finally, we obtain the characteristic SB profile at each redshift bin from the characteristic  $\text{SB}_{\text{Ly}\alpha}^{r=10}$  assuming a power-law profile of  $\text{SB} \propto r^{-2}$  to simplify the calculation. We also confirm that the average SB profile obtained by our method is consistent with the one presented in Borisova et al. (2016). The SB profiles corrected for cosmological dimming are shown as thick blue, cyan and green lines in Figure 6 (right).

iv) For two QSOs at  $z > 6$  with a detected Ly $\alpha$  halo, J2329–0301 and J0305–3150, we estimate  $\text{SB}_{\text{Ly}\alpha}^{r=10}$  by fitting a power law to the data points where Ly $\alpha$  emission is significantly detected, because we find that SB profiles calibrated at  $\text{SB}_{\text{Ly}\alpha}^{r=10}$  slightly overestimate the true profiles. The profiles thus obtained are plotted as thin red and purple lines in Figure 6 (right). The  $\text{SB}_{\text{Ly}\alpha}^{r=10}$  values are  $(6.5 \times 10^{-18}, 3.4 \times 10^{-19}) \text{ erg s}^{-1} \text{ cm}^{-2} \text{ arcsec}^{-2}$  for (J2329–0301, J0305–3150). For the remaining two  $z > 6$  QSOs whose Ly $\alpha$  halos are undetected, we only estimate an upper limit.

We find that the characteristic SB profile clearly decreases with redshift (Figure 6 right), although the sample sizes are still small at  $z > 4$ . The amplitude of the characteristic SB profile at  $z = 2$  is about a factor of 4.0 (16.6) brighter than that at  $z = 3$  ( $z = 4-5$ ). We also compare the SB profiles of the two  $z > 6$  halos with those at lower redshifts. Surprisingly, J2329–0301’s SB is as bright as that of  $z = 2$  halos, while J0305–3150’s SB is even fainter than those at  $z = 4-5$ .

In the optically thin regime of Hennawi & Prochaska (2013) model which appears to be valid for most of our objects, the Ly $\alpha$  SB is proportional to the hydrogen volume density  $n_{\text{H}}$ , the hydrogen total column density  $N_{\text{H}}$ , and the covering factor of clouds in the optically thin CGM  $f_C^{\text{thin}}$  (i.e.,  $\text{SB}_{\text{Ly}\alpha} \propto n_{\text{H}} N_{\text{H}} f_C^{\text{thin}}$ ). Thus, a decrease in the SB am-

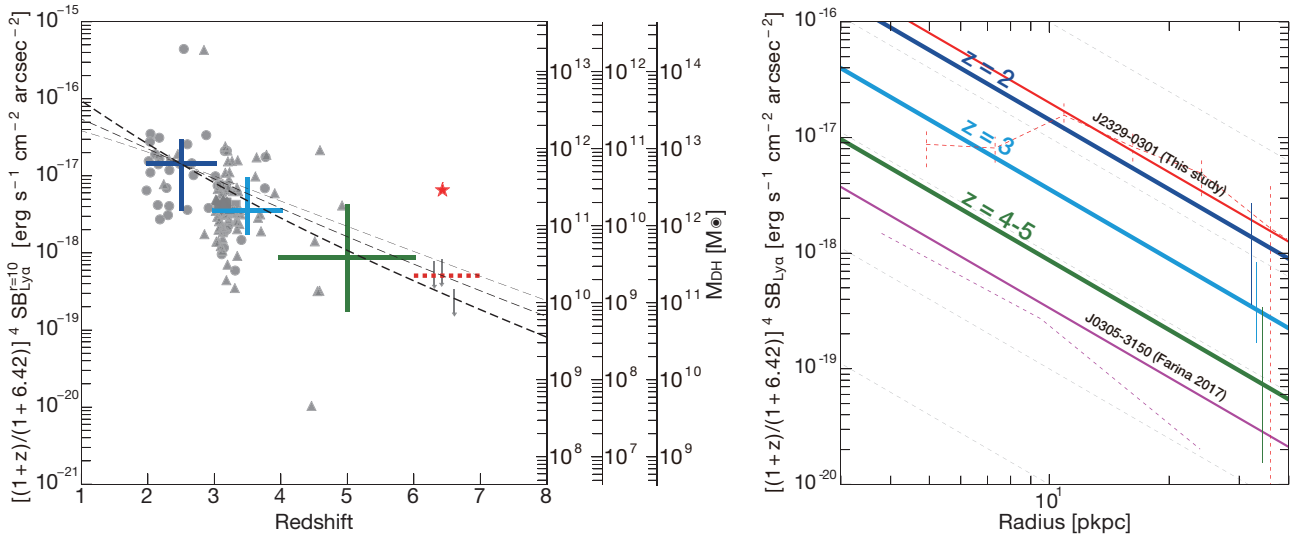


**Figure 6.** (Left)  $SB_{Ly\alpha}^{r=10}$  vs redshift. Colored cross symbols represent median values with errors for  $z = 2, 3$ , and  $4-5$  bins. A dashed red cross is an expected  $SB_{Ly\alpha}^{r=10}$ . Three dashed lines represent  $SB_{Ly\alpha}^{r=10}$  which scales with the mass of dark halos growing up to  $1 \times 10^{11}$  (thin),  $1 \times 10^{12}$  (middle) and  $1 \times 10^{13} M_{\odot}$  (thick) at  $z = 2$ . The ordinate in the right hand side is the dark halo mass calibrated so that  $1 \times 10^{12} M_{\odot}$  corresponds to the median  $SB_{Ly\alpha}^{r=10}$  at  $z = 2$ . (Right) Same as Figure 2, but for median SB profiles derived from median  $SB_{Ly\alpha}^{r=10}$  values on the assumption of  $SB(r) \propto r^{-2}$ : blue,  $z = 2-3$ ; cyan,  $z = 3$ ; green,  $z = 4-5$ . Vertical lines colored in blue, cyan and green are the  $1\sigma$  of the data distributions. Red and purple thin straight lines represent the SB profiles of J2329–0301 and J0305–3150 derived from  $SB_{Ly\alpha}^{r=4}$  and  $SB_{Ly\alpha}^{r=2}$ , respectively, while dashed lines are their original profiles. (A color figure is available in the online journal.)

plitude with redshift implies a decrease in the “hydrogen density”,  $n_H N_H$ , or  $f_C^{\text{thin}}$ , or both. In addition, in the optically thin regime, the total gas mass of the CGM is proportional to  $N_H$  and  $f_C^{\text{thin}}$ . Hence, the decrease in the SB amplitude likely implies a decrease in the total gas mass of the CGM.

#### 5.2.4 The relation between Ly $\alpha$ halo scales and the dark matter halos of hosting QSOs

If the CGM mass around QSOs increases with cosmic time as suggested in Section 5.2.3, what physics causes that? One possibility is the growth of hosting dark matter halos.

Cosmological simulations predict that QSOs at higher- $z$  reside in less massive dark matter halos (e.g., Fanidakis et al. 2012; Oogi et al. 2016). This prediction is also supported by observations (e.g., Eftekharzadeh et al. 2015; He et al. 2018; Uchiyama et al. 2018). Here we use a fitting formula given in Behroozi et al. (2013) to estimate the mass growth rate of QSO hosting halos at  $z > 2$ , assuming that they have grown to  $1 \times 10^{11}$ ,  $1 \times 10^{12}$  or  $1 \times 10^{13} M_{\odot}$  at  $z = 2$ , among which  $1 \times 10^{12} M_{\odot}$  is the closest to the observed values (e.g., Adelberger & Steidel 2005; White et al. 2012). Surprisingly, these halo growth rates, especially those of  $1 \times 10^{12}$  and  $1 \times 10^{13} M_{\odot}$ , are in good agreement with those of  $SB_{Ly\alpha}^{r=10}$ , or the amplitude of the characteristic SB profile: the SB at  $z = 2$  is factors 4.0 and 16.6 higher than those at  $z = 3$  and  $z = 4-5$ , respectively. In other words, the amplitude of the SB scales with the mass of evolving dark matter halos (dashed lines in Figure 6 left). Thus, if the QSOs at different redshifts are on average in a progenitor-descendant relationship in terms of hosting dark matter halos and if the SB amplitude is proportional to the total mass of the CGM,

then the coincidence found here implies that the CGM grows in mass keeping pace with hosting dark matter halos.

We then examine the evolution of the extent of Ly $\alpha$  halos using characteristic SB profiles. We define the extent as the diameter of Ly $\alpha$  halos at a level of  $[(1+z)/(1+6.42)]^4 SB_{Ly\alpha} = 10^{-18} \text{ erg s}^{-1} \text{ cm}^{-2} \text{ arcsec}^{-2}$ , and obtain (76, 38, 20) pkpc for  $z = (2, 3, 4-5)$ . In Figure 7, we compare these characteristic extents with two scaling models. One is  $(1+z)^{-1}$  scaling, i.e., scaling with the virial radius of dark halos with a constant mass (dotted line in Figure 7) as proposed by Ginolfi et al. (2018). The other is  $M_{\text{DH}}^{1/3}(1+z)^{-1}$  scaling, i.e., scaling with the virial radius of evolving dark halos which have  $1 \times 10^{11}$ ,  $1 \times 10^{12}$  or  $1 \times 10^{13} M_{\odot}$  at  $z = 2$ . All models have been calibrated at  $z = 2$ . We find that  $M_{\text{DH}}^{1/3}(1+z)^{-1}$  scaling agrees well with the data, while  $(1+z)^{-1}$  scaling is not steep enough. We stress that the point of our findings here is the assumption that the QSOs in the compilation sample have a progenitor-descendant relationship in terms of hosting dark halos. As shown in Figures 6 (left) and 7, our findings are not sensitive to changes in  $M_{\text{DH}}(z = 2)$ . It is very interesting that the evolution of the SB and extent of Ly $\alpha$  halos can be simultaneously explained by a simple scenario that QSOs are on average in a progenitor-descendant relationship in terms of hosting dark halos and that the mass and size of the CGM just scale with those of hosting halos.

Finally, by extrapolating these evolutionary trends found over  $z \sim 2-5$ , we predict the  $\langle SB_{Ly\alpha}^{r=10} \rangle$  and the characteristic extent for  $z \sim 6$  Ly $\alpha$  halos hosted by progenitors of  $z = 2$  dark halos with  $1 \times 10^{12} M_{\odot}$ . Since the dark halo mass growth rate from  $z = 6$  to  $z = 2$  is calculated to be 31.3 using the formula of Behroozi et al. (2013), we obtain  $\langle SB_{Ly\alpha}^{r=10} \rangle = 4.6 \times 10^{-19} \text{ erg s}^{-1} \text{ cm}^{-2} \text{ arcsec}^{-2}$



and the characteristic extent as 14 pkpc as shown as dotted red symbols in Figures 6 (left) and 7. These values are comparable to those of J0305–3150, but much lower than those of J2329–0301. This may suggest that J2329–0301 is a rare QSO which has an exceptionally bright Ly $\alpha$  halo, although a statistically meaningful comparison requires a much larger sample.

### 5.2.5 Systematic uncertainties and biases that could cause a redshift evolution of QSOs' Ly $\alpha$ halos

In this subsection, we discuss systematic uncertainties and biases that could produce (part of) the observed decline of  $SB_{Ly\alpha}^{r=10}$  (Section 5.2.3). Four candidates are discussed.

The first one is underestimation of  $L_{Ly\alpha}$ . The Ly $\alpha$  fluxes of halos in our compilation sample have been measured by either slit spectroscopy or imaging (including integral field unit or integral field spectroscopy); those from slit spectroscopy are fainter than total Ly $\alpha$  fluxes because of slit loss. Although the original papers have given slit-loss corrected Ly $\alpha$  fluxes, those corrections may be insufficient. For instance, we find that J2329–0301's  $L_{Ly\alpha}$  derived from spectroscopic observations in Willott et al. (2011) is smaller than our estimate by a factor of 1.2. If such underestimation is present in our compilation sample, the *true* characteristic median of  $\langle SB_{Ly\alpha}^{r=10} \rangle$  should be larger than our estimates. In particular, the  $L_{Ly\alpha}$  of most of the  $z = 4 - 5$  halos have been measured by slit spectroscopy. Thus, we evaluate the sensitiveness of  $\langle SB_{Ly\alpha}^{r=10} \rangle$  to the slit-loss correction factor of those  $z = 4 - 5$  halos. We find that the  $\langle SB_{Ly\alpha}^{r=10} \rangle$  at  $z = 4 - 5$  becomes as bright as the  $z = 3$  value if their *true*  $L_{Ly\alpha}$  were larger by about a factor of 10. Such a large amount of slit loss appears to be unrealistic.

The second candidate is a possible lack of ELAN-like halos at  $z = 4 - 5$ . At  $z = 2 - 3$ , extremely bright and extended Ly $\alpha$  halos have been found around some QSOs, and are called ELAN (Enourmous Lyman-Alpha Nebulae; Cantalupo et al. 2014; Hennawi et al. 2015; Cai et al. 2017, 2018; Arrigoni Battaia et al. 2019, 2018). Current statistics of the detection probability of ELAN suggest its rareness of only a few percent of QSOs at  $z \sim 3$  (Arrigoni Battaia et al. 2019). If ELAN were similarly rare at  $z = 4 - 5$  and our compilation sample misses such ELAN-like halos, our  $\langle SB_{Ly\alpha}^{r=10} \rangle$  value would be biased low. To examine the effect of ELAN on  $\langle SB_{Ly\alpha}^{r=10} \rangle$  estimates, we exclude ELAN from our compilation sample, and derive  $\langle SB_{Ly\alpha}^{r=10} \rangle$ . The  $\langle SB_{Ly\alpha}^{r=10} \rangle$  values thus obtained are  $(1.4 \times 10^{-17}, 3.5 \times 10^{-18}, 8.7 \times 10^{-19})$  erg s $^{-1}$  cm $^{-2}$  arcsec $^{-2}$  for  $z = (2, 3, 4 - 5)$ ; the differences from the original values are very small. Thus, the presence of ELAN has negligible effects on our results.

Our SB and size estimates will also be biased low if our sample misses relatively large Ly $\alpha$  halos with  $d > 100$  pkpc at  $z > 4$ . Indeed, radio-quiet QSOs at  $z \sim 2$  are known to possess no or only a small halo with  $d < 50$  pkpc (e.g. Herenz et al. 2015; Arrigoni Battaia et al. 2016), and all the  $z = 4 - 5$  objects in our sample are radio-quiet (see also Figure 6 left). However, currently there is no observation that suggests  $z = 4 - 5$  QSOs to have similar radio-loudness dependence. A larger sample including radio-loud QSOs is needed for further discussion.

The third candidate is a small sample size at  $z = 4 - 5$ . Our  $\langle SB_{Ly\alpha}^{r=10} \rangle$  value at this redshift bin is derived from only

six QSOs, which are much fewer than those at  $z = 2$  and 3. Our  $z = 4 - 5$  sample may be greatly underestimating the true  $\langle SB_{Ly\alpha}^{r=10} \rangle$  owing to large statistical fluctuations. However, we cannot test this possibility by our sample. A larger sample is needed to do so.

Finally, we discuss the possibility that the decreasing trend of  $\langle SB_{Ly\alpha}^{r=10} \rangle$  is not a common feature of all QSOs but seen only in those satisfying our selection criteria. Because the purpose of this study is to investigate correlations between Ly $\alpha$  halo properties and hosting QSOs' physical parameters, we do not include QSOs whose halo is either undetected or too small (diameter  $< 20$  pkpc) to define  $SB_{Ly\alpha}^{r=10}$  (see also Section 5.2.3). In this respect, our results are biased. However, Arrigoni Battaia et al. (2019) have found an opposite trend that the SB at  $z = 2$  is a factor of 10 fainter than that at  $z = 3$  when they have included in the  $z = 2$  sample those with an undetected or small Ly $\alpha$  halos. In fact, not all  $z = 2$  QSOs have Ly $\alpha$  halos, with detection rates of about 30 – 70% (e.g., Lehnert et al. 1999; Heckman et al. 1991b; Hennawi & Prochaska 2013; Arrigoni Battaia et al. 2016). Including such QSOs in our sample should naturally reduce the median SB. However, it is not straightforward to estimate the degree of the reduction, because Arrigoni Battaia et al. (2019) have not included large detected Ly $\alpha$  halos at  $z = 2$ . In addition, non-detected Ly $\alpha$  halos may also be present at  $z = 4 - 5$  and may similarly reduce the median SB there. Tracing the Ly $\alpha$  halo evolution of the entire QSO population needs an unbiased survey like the QSO MUSEUM (Quasar Snapshot Observations with MUSE: Search for Ex-tended Ultraviolet eMission: Arrigoni Battaia et al. 2019) over a wide redshift range.

## 6 SUMMARY

In this paper, we have first investigated the very luminous Ly $\alpha$  halo around the QSO J2329–0301 at  $z = 6.42$  with new data. Then, we have systematically studied the properties of QSO Ly $\alpha$  halos over  $z \sim 2 - 6$  using all available data in the literature ('compilation sample'). The major results are summarized below.

1. We have confirmed extended Ly $\alpha$  emission around J2329–0301, with a Ly $\alpha$  luminosity of  $9.8 \times 10^{43}$  erg s $^{-1}$  within an extent of  $\sim 37$  pkpc. The SB of this halo is about an order of magnitude brighter than that of another halo-detected QSO at  $z > 6$ , QSO J0305–3150, but comparable to those of luminous halos at  $z \sim 3$  (Borisova et al. 2016).

2. We have examined correlations of several parameters characterizing Ly $\alpha$  halos with [1] redshift, [2]  $M_{BH}$  the Eddington ratio, and  $L_{BoI}$  and [3] spectral index  $\alpha$  and IRX among the compilation sample.

[ 1 ] We have found declines of  $L_{Ly\alpha}$ ,  $L_{Ly\alpha}/L_{BoI}$  and  $d$  with redshift, indicating some redshift evolution of Ly $\alpha$  halos.

[ 2 ] We have found a strong positive correlation between  $L_{Ly\alpha}$  vs.  $d$  and a moderate correlation between  $d$  vs.  $L_{Ly\alpha}/L_{BoI}$  based on Spearman's test. A possible negative trend has also been seen in the  $d$  vs.  $M_{BH}$  and  $d$  vs.  $L_{Ly\alpha}/L_{BoI}$  distributions when limited to  $z > 6$ .

[ 3 ] Spearman's test has also indicated a moderate negative correlation of  $d$  and  $L_{Ly\alpha}/L_{BoI}$  with the IRX, al-

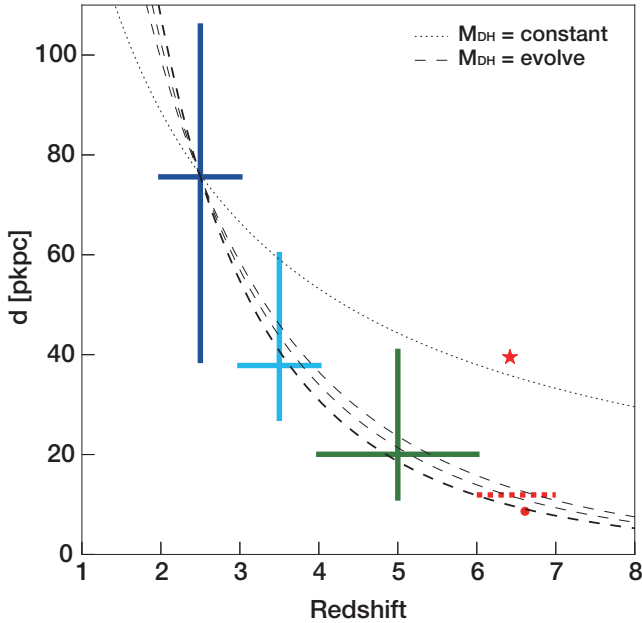


**Figure 7.** Extent of Ly $\alpha$  halos as a function redshift. Colored cross symbols represent the characteristic extents at  $z = 2, 3, 4-5$  defined as the diameter of halos at  $[(1+z)/(1+6.42)]^4 \text{SB}_{\text{Ly}\alpha} = 10^{-18} \text{ erg s}^{-1} \text{ cm}^{-2} \text{ arcsec}^{-2}$ . Because the characteristic extent at  $z = 6$  is a prediction, it is plotted with a dotted line. A star and a circle represent the extents of J2329–0301 and J0305–3150, respectively. A dotted line shows scaling with  $(1+z)^{-1}$ , while three dashed lines are scaling with  $M_{\text{DH}}^{1/3}(1+z)^{-1}$  as in the case of Figure 6 (left). (A color figure is available in the online journal.)

though the errors in the  $\rho$  parameter are large due to a very small sample size. These trends become relatively clearer when the sample is limited to  $z > 6$ .

3. We have examined physical properties of four  $z > 6$  QSOs which have a wide range of  $L_{\text{Ly}\alpha}$ . We have found that the dust content probably controls the presence/absence of Ly $\alpha$  halos because QSOs with no or a small Ly $\alpha$  halo have a higher IR luminosity and dust mass than J2329–0301 which has an extraordinarily luminous and extended Ly $\alpha$  halo. J2329–0301 also has the least massive  $M_{\text{BH}}$  ( $M_{\text{BH}} < 10^9 M_{\odot}$ ) among the four. We infer that QSOs have a Ly $\alpha$  halo only in the young phase because those in older phases have a large amount of dust which absorbs ionizing photons before escaping out to circum-galactic regions.

4. The Ly $\alpha$  halo around J2329–0301 is optically thin against ionizing photons. It is also found that at least  $\sim 88\%$  of the compilation sample are optically thin.

5. We have derived the characteristic SB profile at  $z = 2, 3$ , and  $4-5$  from the SB at 10 pkpc radius ( $\text{SB}_{\text{Ly}\alpha}^{r=10}$ ) with an assumption of a universal power-law profile of  $\text{SB} \propto r^{-2}$ , and then, found that  $\text{SB}_{\text{Ly}\alpha}^{r=10}$  increases with cosmic time. Its growth rate between  $z = 2$  and  $z = 3$  ( $z = 4-5$ ) is a factor of 4.0 (16.6). Because the SB is proportional to “hydrogen density ( $n_{\text{H}}N_{\text{H}}$ )” and  $f_{\text{C}}^{\text{thin}}$ , and the total gas mass of the CGM scales with these parameters, the brightening of the SB likely indicates an increase in the CGM gas mass with time. The increasing rate of the SB coincides with the mass growth rate of dark halos that evolve to  $1 \times 10^{12}$  or  $1 \times 10^{13} M_{\odot}$  at  $z = 2$ .

6. We have also estimated the characteristic extents of Ly $\alpha$  halos to be (76, 38, 20) pkpc for  $z = (2, 3, 4-5)$ . The evolution of the characteristic extent does not match  $(1+z)^{-1}$  scaling which is suggested by Ginolfi et al. (2018), but matches well  $M_{\text{DH}}^{1/3}(1+z)^{-1}$  scaling, i.e., scaling with the virial radius of evolving dark halos. These increases in SB and extent with time are consistent with a scenario that the CGM around QSOs evolves in mass and size keeping pace with hosting dark matter halos.

7. Extrapolating these evolutionary trends, we have predicted the mean  $\text{SB}_{\text{Ly}\alpha}^{r=10}$  and extent for  $z = 6$  Ly $\alpha$  halos to be  $\langle \text{SB}_{\text{Ly}\alpha}^{r=10} \rangle = 4.6 \times 10^{-19} \text{ erg s}^{-1} \text{ cm}^{-2} \text{ arcsec}^{-2}$  and 14 pkpc. These values are comparable to those of J0305–3150, but much lower than those of J2329–0301, indicating a rareness of J2329–0301’s Ly $\alpha$  halo.

## ACKNOWLEDGEMENTS

We appreciate the referee and the editor for providing the constructive suggestions and comments to improve our manuscript. We are grateful to E. P. Farina and F. Arrigoni Battaia for providing the data of Farina et al. (2017) and Arrigoni Battaia et al. (2019), and S. Cantalupo, G. Pezzulli and E. Borisova for providing the data of Borisova et al. (2016). We thank M. Rauch, Z. Cai, J. X. Prochaska, K. Inayoshi, M. Onoue, T. Oogi, H. Kusakabe, T. Okamura, S. Mukae, and M. Ando for helpful discussions. We acknowledge grant aid for the narrow band filter from the Department of Astronomical Sciences of the Graduate University for Advanced Studies (SOKENDAI). RM acknowledges a Japan Society for the Promotion of Science (JSPS) Fellowship at Japan and a Ministry of Science and Technology (MOST) Fellowship at Taiwan. RM was supported by JSPS KAKENHI 18J40088, and by MOST grant 104-2112-M-007-021-MY3. YU was supported by JSPS KAKENHI Grant Number JP26800103, JP24103003. TG acknowledges support by the Ministry of Science and Technology of Taiwan through grant 105-2112-M-007-003-MY3.

## REFERENCES

- Adelberger K. L., Steidel C. C., 2005, *ApJ*, **630**, 50
- Alam S. M. K., Miralda-Escudé J., 2002, *ApJ*, **568**, 576
- Arrigoni Battaia F., Hennawi J. F., Cantalupo S., Prochaska J. X., 2016, *ApJ*, **829**, 3
- Arrigoni Battaia F., Prochaska J. X., Hennawi J. F., Obreja A., Buck T., Cantalupo S., Dutton A. A., Macciò A. V., 2018, *MNRAS*, **473**, 3907
- Arrigoni Battaia F., Hennawi J. F., Prochaska J. X., Oñorbe J., Farina E. P., Cantalupo S., Lusso E., 2019, *MNRAS*, **482**, 3162
- Bañados E., et al., 2016, *ApJS*, **227**, 11
- Bacon R., et al., 2015, *A&A*, **575**, A75
- Barkana R., Loeb A., 2001, *Phys. Rep.*, **349**, 125
- Barrio F. E., et al., 2008, *MNRAS*, **389**, 792
- Bayliss M. B., et al., 2017, *ApJ*, **845**, L14
- Behroozi P. S., Wechsler R. H., Conroy C., 2013, *ApJ*, **770**, 57
- Bergeron J., Petitjean P., Cristiani S., Arnouts S., Bresolin F., Fasano G., 1999, *A&A*, **343**, L40
- Bernstein R. A., 2007, *ApJ*, **666**, 663
- Borisova E., et al., 2016, *ApJ*, **831**, 39

- Bouché N., Murphy M. T., Kacprzak G. G., Péroux C., Con-  
tini T., Martin C. L., Dessauges-Zavadsky M., 2013, *Science*,  
341, 50
- Bouché N., et al., 2016, *ApJ*, 820, 121
- Bremer M. N., Fabian A. C., Sargent W. L. W., Steidel C. C.,  
Boksenberg A., Johnstone R. M., 1992, *MNRAS*, 258, 23P
- Bunker A., Smith J., Spinrad H., Stern D., Warren S., 2003,  
*Ap&SS*, 284, 357
- Cai Z., et al., 2017, *ApJ*, 837, 71
- Cai Z., et al., 2018, *ApJ*, 861, L3
- Calura F., Gilli R., Vignali C., Pozzi F., Pipino A., Matteucci F.,  
2014, *MNRAS*, 438, 2765
- Cantalupo S., Porciani C., Lilly S. J., Miniati F., 2005, *ApJ*,  
628, 61
- Cantalupo S., Arrigoni-Battaia F., Prochaska J. X., Hennawi  
J. F., Madau P., 2014, *Nature*, 506, 63
- Christensen L., Jahnke K., Wisotzki L., Sánchez S. F., 2006,  
*A&A*, 459, 717
- Courbin F., North P., Eigenbrod A., Chelouche D., 2008, *A&A*,  
488, 91
- Davé R., Oppenheimer B. D., Finlator K., 2011, *MNRAS*, 415, 11
- De Rosa G., et al., 2014, *ApJ*, 790, 145
- Decarli R., et al., 2012, *ApJ*, 756, 150
- Decarli R., et al., 2018, *ApJ*, 854, 97
- Dekel A., et al., 2009a, *Nature*, 457, 451
- Dekel A., Sari R., Ceverino D., 2009b, *ApJ*, 703, 785
- Dijkstra M., Kramer R., 2012, *MNRAS*, 424, 1672
- Eftekharzadeh S., et al., 2015, *MNRAS*, 453, 2779
- Fanidakis N., et al., 2012, *MNRAS*, 419, 2797
- Farina E. P., Falomo R., Decarli R., Treves A., Kotilainen J. K.,  
2013, *MNRAS*, 429, 1267
- Farina E. P., Falomo R., Scarpa R., Decarli R., Treves A., Koti-  
lainen J. K., 2014, *MNRAS*, 441, 886
- Farina E. P., et al., 2017, *ApJ*, 848, 78
- Fathivavari H., Petitjean P., Noterdaeme P., Pâris I., Finley H.,  
López S., Srianand R., 2016, *MNRAS*, 461, 1816
- Feldmeier J. J., et al., 2013, *ApJ*, 776, 75
- Francis P. J., McDonnell S., 2006, *MNRAS*, 370, 1372
- Fumagalli M., Cantalupo S., Dekel A., Morris S. L., O’Meara  
J. M., Prochaska J. X., Theuns T., 2016, *MNRAS*, 462, 1978
- Fynbo J. U., Thomsen B., Møller P., 2000, *A&A*, 353, 457
- Ginolfi M., Maiolino R., Carniani S., Arrigoni Battaia F., Can-  
talupo S., Schneider R., 2018, *MNRAS*, 476, 2421
- Goto T., Utsumi Y., Furusawa H., Miyazaki S., Komiyama Y.,  
2009, *MNRAS*, 400, 843
- Goto T., Utsumi Y., Walsh J. R., Hattori T., Miyazaki S., Ya-  
mauchi C., 2012, *MNRAS*, 421, L77
- Goto T., Utsumi Y., Kikuta S., Miyazaki S., Shiki K., Hashimoto  
T., 2017, *MNRAS*, 470, L117
- Gould A., Weinberg D. H., 1996, *ApJ*, 468, 462
- Graham A. W., Scott N., 2013, *ApJ*, 764, 151
- Gunn J. E., Stryker L., 1983, *Stellar spectrometric atlas 3130 A*  
- 10800 A
- Haiman Z., Rees M. J., 2001, *ApJ*, 556, 87
- Hayes M., et al., 2013, *ApJ*, 765, L27
- He W., et al., 2018, *PASJ*, 70, S33
- Heckman T. M., Lehnert M. D., van Breugel W., Miley G. K.,  
1991a, *ApJ*, 370, 78
- Heckman T. M., Lehnert M. D., Miley G. K., van Breugel W.,  
1991b, *ApJ*, 381, 373
- Hennawi J. F., Prochaska J. X., 2013, *ApJ*, 766, 58
- Hennawi J. F., et al., 2006, *ApJ*, 651, 61
- Hennawi J. F., Prochaska J. X., Cantalupo S., Arrigoni-Battaia  
F., 2015, *Science*, 348, 779
- Herenz E. C., Wisotzki L., Roth M., Anders F., 2015, *A&A*,  
576, A115
- Hogan C. J., Weymann R. J., 1987, *MNRAS*, 225, 1P
- Hopkins P. F., Hernquist L., Cox T. J., Kereš D., 2008, *ApJS*,  
175, 356
- Hughes D. H., Dunlop J. S., Rawlings S., 1997, *MNRAS*, 289, 766
- Humphrey A., Binette L., Villar-Martín M., Aretxaga I., Pa-  
paderos P., 2013, *MNRAS*, 428, 563
- Husband K., Bremer M. N., Stanway E. R., Lehnert M. D., 2015,  
*MNRAS*, 452, 2388
- Jiang L., et al., 2006, *AJ*, 132, 2127
- Jiang L., Fan X., Vestergaard M., Kurk J. D., Walter F., Kelly  
B. C., Strauss M. A., 2007, *AJ*, 134, 1150
- Johnson S. D., Chen H.-W., Mulchaey J. S., 2015, *MNRAS*,  
452, 2553
- Kikuta S., Imanishi M., Matsuoka Y., Matsuda Y., Shimasaku  
K., Nakata F., 2017, *ApJ*, 841, 128
- King I. R., 1971, *PASP*, 83, 199
- Kollmeier J. A., Zheng Z., Davé R., Gould A., Katz N., Miralda-  
Escudé J., Weinberg D. H., 2010, *ApJ*, 708, 1048
- Kormendy J., Ho L. C., 2013, *ARA&A*, 51, 511
- Kozłowski S., 2017, *ApJS*, 228, 9
- Lau M. W., Prochaska J. X., Hennawi J. F., 2016, *ApJS*, 226, 25
- Laursen P., Sommer-Larsen J., 2007, *ApJ*, 657, L69
- Laursen P., Sommer-Larsen J., Andersen A. C., 2009, *ApJ*,  
704, 1640
- Leclercq F., et al., 2017, *A&A*, 608, A8
- Lehnert M. D., Becker R. H., 1998, *A&A*, 332, 514
- Lehnert M. D., van Breugel W. J. M., Heckman T. M., Miley  
G. K., 1999, *ApJS*, 124, 11
- Leipski C., et al., 2014, *ApJ*, 785, 154
- Lu Y., Yu Q., 1999, *ApJ*, 526, L5
- Lusso E., Worseck G., Hennawi J. F., Prochaska J. X., Vignali  
C., Stern J., O’Meara J. M., 2015, *MNRAS*, 449, 4204
- Lyu J., Rieke G. H., Alberts S., 2016, *ApJ*, 816, 85
- Ma Z., Yan H., 2015, *ApJ*, 811, 58
- Magorrian J., et al., 1998, *AJ*, 115, 2285
- Marconi A., Hunt L. K., 2003, *ApJ*, 589, L21
- Martin D. C., Chang D., Matuszewski M., Morrissey P., Rahman  
S., Moore A., Steidel C. C., 2014, *ApJ*, 786, 106
- Matsuda Y., et al., 2011, *MNRAS*, 410, L13
- Matsuda Y., et al., 2012, *MNRAS*, 425, 878
- Mazzucchelli C., et al., 2017, *ApJ*, 849, 91
- McLure R. J., Dunlop J. S., 2002, *MNRAS*, 331, 795
- Merritt D., Ferrarese L., 2001, *ApJ*, 547, 140
- Miyazaki S., et al., 2002, *PASJ*, 54, 833
- Moffat A. F. J., 1969, *A&A*, 3, 455
- Momose R., et al., 2014, *MNRAS*, 442, 110
- Momose R., et al., 2016, *MNRAS*, 457, 2318
- Mori M., Umemura M., 2006, *Nature*, 440, 644
- Mori M., Ferrara A., Madau P., 2002, *ApJ*, 571, 40
- Mori M., Umemura M., Ferrara A., 2004, *ApJ*, 613, L97
- Murphy M. T., Bernet M. L., 2016, *MNRAS*, 455, 1043
- North P. L., Courbin F., Eigenbrod A., Chelouche D., 2012, *A&A*,  
542, A91
- North P. L., et al., 2017, *A&A*, 604, A23
- Oogi T., Enoki M., Ishiyama T., Kobayashi M. A. R., Makiya R.,  
Nagashima M., 2016, *MNRAS*, 456, L30
- Pâris I., et al., 2014, *A&A*, 563, A54
- Pâris I., et al., 2017, *A&A*, 597, A79
- Pentericci L., et al., 2003, *A&A*, 410, 75
- Prochaska J. X., Hennawi J. F., 2009, *ApJ*, 690, 1558
- Prochaska J. X., et al., 2013a, *ApJ*, 776, 136
- Prochaska J. X., et al., 2013b, *ApJ*, 776, 136
- Prochaska J. X., Lau M. W., Hennawi J. F., 2014, *ApJ*, 796, 140
- Prochaska J. X., et al., 2017, *ApJ*, 837, 169
- Racine R., 1996, *PASP*, 108, 699
- Rauch M., et al., 2008, *ApJ*, 681, 856
- Rauch M., Becker G. D., Haehnelt M. G., Carswell R. F., Gauthier  
J.-R., 2013, *MNRAS*, 431, L68
- Rees M. J., 1988, *MNRAS*, 231, 91p

- Richards G. T., et al., 2006, [ApJS](#), **166**, 470
- Roche N., Humphrey A., Binette L., 2014, [MNRAS](#), **443**, 3795
- Roettgering H. J. A., van Ojik R., Miley G. K., Chambers K. C., van Breugel W. J. M., de Koff S., 1997, [A&A](#), **326**, 505
- Scannapieco E., Silk J., Bouwens R., 2005, [ApJ](#), **635**, L13
- Shen Y., Greene J. E., Strauss M. A., Richards G. T., Schneider D. P., 2008, [ApJ](#), **680**, 169
- Shen Y., et al., 2011, [ApJS](#), **194**, 45
- Shimasaku K., Ouchi M., Furusawa H., Yoshida M., Kashikawa N., Okamura S., 2005, [PASJ](#), **57**, 447
- Smith D. J. B., Jarvis M. J., Simpson C., Martínez-Sansigre A., 2009, [MNRAS](#), **393**, 309
- Steidel C. C., Sargent W. L. W., Dickinson M., 1991, [AJ](#), **101**, 1187
- Steidel C. C., Bogosavljević M., Shapley A. E., Kollmeier J. A., Reddy N. A., Erb D. K., Pettini M., 2011, [ApJ](#), **736**, 160
- Trainor R., Steidel C. C., 2013, [ApJ](#), **775**, L3
- Tsai C.-W., et al., 2015, [ApJ](#), **805**, 90
- Uchiyama H., et al., 2018, [PASJ](#), **70**, S32
- Utsumi Y., Goto T., Kashikawa N., Miyazaki S., Komiyama Y., Furusawa H., Overzier R., 2010, [ApJ](#), **721**, 1680
- Venemans B. P., Walter F., Zschaechner L., Decarli R., De Rosa G., Findlay J. R., McMahon R. G., Sutherland W. J., 2016, [ApJ](#), **816**, 37
- Verhamme A., Dubois Y., Blaizot J., Garel T., Bacon R., Devriendt J., Guiderdoni B., Slyz A., 2012, [A&A](#), **546**, A111
- Vestergaard M., 2003, [ApJ](#), **599**, 116
- Vestergaard M., Osmer P. S., 2009, [ApJ](#), **699**, 800
- Weedman D., Sargsyan L., Lebouteiller V., Houck J., Barry D., 2012, [ApJ](#), **761**, 184
- Weidinger M., Møller P., Fynbo J. P. U., 2004, [Nature](#), **430**, 999
- White M., et al., 2012, [MNRAS](#), **424**, 933
- Willott C. J., et al., 2007, [AJ](#), **134**, 2435
- Willott C. J., et al., 2010, [AJ](#), **140**, 546
- Willott C. J., Chet S., Bergeron J., Hutchings J. B., 2011, [AJ](#), **142**, 186
- Willott C. J., Omont A., Bergeron J., 2013, [ApJ](#), **770**, 13
- Willott C. J., Bergeron J., Omont A., 2017, [ApJ](#), **850**, 108
- Wisotzki L., et al., 2016, [A&A](#), **587**, A98
- Yajima H., Sugimura K., Hasegawa K., 2018, [MNRAS](#), **477**, 5406
- Yang Y., Zabludoff A., Tremonti C., Eisenstein D., Davé R., 2009, [ApJ](#), **693**, 1579
- van Ojik R., Roettgering H. J. A., Miley G. K., Hunstead R. W., 1997, [A&A](#), **317**, 358